

A process-based analysis of ocean heat uptake in an AOGCM with an eddy-permitting ocean component

Article

Accepted Version

Kuhlbrodt, T. ORCID: <https://orcid.org/0000-0003-2328-6729>, Gregory, J. ORCID: <https://orcid.org/0000-0003-1296-8644> and Shaffrey, L. ORCID: <https://orcid.org/0000-0003-2696-752X> (2015) A process-based analysis of ocean heat uptake in an AOGCM with an eddy-permitting ocean component. *Climate Dynamics*, 45 (11). pp. 3205-3226. ISSN 1432-0894 doi: 10.1007/s00382-015-2534-0 Available at <https://centaur.reading.ac.uk/39329/>

It is advisable to refer to the publisher's version if you intend to cite from the work. See [Guidance on citing](#).

To link to this article DOI: <http://dx.doi.org/10.1007/s00382-015-2534-0>

Publisher: Springer

All outputs in CentAUR are protected by Intellectual Property Rights law, including copyright law. Copyright and IPR is retained by the creators or other copyright holders. Terms and conditions for use of this material are defined in the [End User Agreement](#).

www.reading.ac.uk/centaur

CentAUR

Central Archive at the University of Reading

Reading's research outputs online

Climate Dynamics manuscript No. (will be inserted by the editor)

A process-based analysis of ocean heat uptake in an AOGCM with an eddy-permitting ocean component

T. Kuhlbrodt · J. M. Gregory · L. C. Shaffrey

Received: date / Accepted: date

Abstract About 90% of the anthropogenic increase in heat stored in the climate system is found the oceans. Therefore it is relevant to understand the details of ocean heat uptake. Here we present a detailed, process-based analysis of ocean heat uptake (OHU) processes in HiGEM1.2, an atmosphere-ocean general circulation model (AOGCM) with an eddy-permitting ocean component of $1/3^\circ$ resolution. Similarly to various other models, HiGEM1.2 shows that the global heat budget is dominated by a downward advection of heat compensated by upward isopycnal diffusion. Only in the upper tropical ocean do we find the classical balance between downward diapycnal diffusion and upward advection of heat. The upward isopycnal diffusion of heat is located mostly in the Southern Ocean, which thus dominates the global heat budget. We compare the responses to a $4\times\text{CO}_2$ forcing and an enhancement of the windstress forcing in the Southern Ocean. This highlights the importance of regional processes for the global ocean heat uptake. These are mainly surface fluxes and convection in the high latitudes, and advection in the Southern Ocean mid-latitudes. Changes in diffusion are less important. In line with the CMIP5 models, HiGEM1.2 shows a band of strong OHU in the mid-latitude Southern Ocean in the $4\times\text{CO}_2$ run, which is mostly advective. By contrast, in the high-latitude Southern Ocean regions it is the suppression of convection that leads to OHU. In the enhanced windstress run, convection is strengthened at high Southern latitudes, leading to heat loss, while the magnitude of the OHU in the Southern mid-latitudes is very similar to the $4\times\text{CO}_2$ results. Remarkably, there is only very small global OHU in the enhanced windstress run. The wind stress forcing just leads to a redistribution of heat. We relate the ocean changes at high southern latitudes to the effect of climate change on the Antarctic Circumpolar Current (ACC). It weakens in the $4\times\text{CO}_2$ run and strengthens in the wind stress run. The weakening is due to a narrowing of the ACC, caused by an expansion of the Weddell Gyre, and a flattening of the isopycnals, which are explained by a combination of the wind stress forcing and increased precipitation.

T. Kuhlbrodt, J. M. Gregory and L. C. Shaffrey
NCAS, Department of Meteorology
University of Reading
Earley Gate, PO Box 243
Reading RG6 6BB, UK E-mail: t.kuhlbrodt@reading.ac.uk

J. M. Gregory
Met Office Hadley Centre
Exeter, UK

31 **Keywords** Ocean heat uptake · Process-based analysis · Advection-diffusion balance ·
 32 Isopycnal diffusion · Eddy-permitting ocean model · Southern Ocean · Antarctic
 33 Circumpolar Current

34 1 Introduction

35 Ocean heat uptake leads to thermal expansion of the sea water, which is one of the main
 36 causes of sea level rise globally (Church et al, 2011). Therefore, understanding ocean heat
 37 uptake (OHU) processes helps to reduce the large uncertainty exhibited by contemporary cli-
 38 mate models in projections of future sea level change, especially on regional scales (Yin et al,
 39 2010; Pardaens et al, 2011; Yin, 2012; Bouttes et al, 2012). Due to a lack of process-based
 40 observations with a global coverage, models are valuable for the analysis of ocean heat up-
 41 take processes. On a global scale, Gregory and Forster (2008) and Dufresne and Bony (2008)
 42 analysed the spread of atmosphere-ocean general circulation models (AOGCMs; used for the
 43 Coupled Model Intercomparison Project 3 [CMIP3]) in terms of ocean heat uptake under an
 44 idealized CO₂ increase, however without analysing the OHU processes in detail. Kuhlbrodt
 45 and Gregory (2012) similarly analysed the CMIP5 models. They found that most models
 46 have a vertical temperature gradient that is too weak, suggesting an over-estimate of ocean
 47 heat uptake. Their analysis also revealed that the ocean heat uptake efficiency varies by a
 48 factor of 2 across the models.

49 To make further progress with identifying the sources of the model spread and model
 50 biases revealed by these intercomparisons, more detailed, i.e. process-based analyses are re-
 51 quired, employing the individual terms in the temperature tendency equation like advection,
 52 the different kinds of diffusion, convection, or ice physics.

53 1.1 Definitions

54 Before we proceed to a discussion of the previous work in this field we need to clearly
 55 define the terms we will use. We find that in the literature there is some ambiguity about
 56 which OHU processes are called “advective” and “diffusive”. This warrants clarification.
 57 There are different ways to define these two terms. In the real ocean, almost all processes
 58 that distribute heat are advective, from large-scale currents and mesoscale eddies through to
 59 local small-scale turbulence. In this view, the only properly diffusive process is molecular
 60 diffusion. In a given ocean model however, the OHU processes fall first of all into two
 61 categories, “resolved” and “unresolved”. A subset of the unresolved processes is covered by
 62 parameterizations; these processes are thus often called “parameterized”. Obviously, these
 63 categories are a function of the model’s grid scale. Processes that are resolved in model
 64 A might be parameterized in model B. There is also a tendency to call, in models, resolved
 65 processes “advective” and parameterized processes “diffusive”. This arises because resolved
 66 processes are captured by the model’s advection scheme, and because many sub-gridscale
 67 processes are parameterized as diffusion.

68 It follows that the labels “advective” and “diffusive” depend on the model’s grid scale.
 69 This makes a comparison of models with different grid scale difficult, since these labels are
 70 not consistently defined across models. We will discuss an example below: whether we call
 71 mesoscale eddy-induced heat transports “advective” or “diffusive” is a matter of interpreta-
 72 tion. For another example, a model with a grid scale of 0.1° might not need a parameteriza-
 73 tion for isopycnal mixing or eddy-induced mixing because its advection contains all these

processes. On the other hand, a model with a grid scale of 1° will have parameterisations for these processes, and its advection contains only the large-scale processes. But even in models with very similar grid scales, the use (or not) of parameterisations may differ.

The advective processes can be decomposed. For the temperature change in a high-resolution (say, 0.1°) ocean model due to advection $\nabla \cdot \bar{\mathbf{v}}\bar{T}$, we use the customary Reynolds decomposition into a mean part and an eddy part: $\nabla \cdot (\bar{\mathbf{v}}\bar{T}) = \nabla \cdot (\bar{\mathbf{v}}\bar{T}) + \nabla \cdot \bar{\mathbf{v}}'\bar{T}'$. Herein, \mathbf{v} is the three-dimensional resolved velocity, T is the temperature, the overbar denotes a temporal average and the prime the deviation from this average. The Reynolds eddy part actually contains any kind of transient variability. The sum of the temperature change due to the mean advection and the temperature change due to the eddy advection is called here the temperature change due to the *residual* advection. The residual advection is equivalent to the resolved advection in high-resolution models.

In the literature, this decomposition of the advective temperature change is used with ocean models that are eddy-permitting or high-resolution (e.g. Wolfe et al, 2008; Morrison et al, 2013, and this study), where “eddy” now rather refers to mesoscale eddies. If ocean models with a coarser resolution are analysed (typically 1° or larger), then this decomposition is not made and $\nabla \cdot \bar{\mathbf{v}}\bar{T}$ change is simply called “advective” (Brierley et al, 2010) or “resolved advective heat flux” (Hieronymus and Nycander, 2013).

In coarser resolution models, usually a parameterization of the eddy advective heat transport is used, based on Gent and McWilliams (1990). This temperature change due to parameterized eddy advection is often called “GM flux” (Brierley et al, 2010). It should not be confused with the temperature change due to resolved eddy advection, as defined above.

In coarser resolution models as well as in some eddy-permitting models (resolution of $1/3^\circ$ or $1/4^\circ$), often a parameterization of isopycnal mixing is used, too. Examples of eddy-permitting models using an isopycnal diffusion parameterization are this study and NEMO in the $1/4^\circ$ configuration used for the UK Met Office climate models (Megann et al, 2014). Examples of eddy-permitting models not using an isopycnal diffusion parameterization are Wolfe et al (2008); Morrison et al (2013) and Griffies et al (2015). In the latter models it is assumed that the resolved advection by the “permitted” eddies leads to sufficient mixing along isopycnals. However, in some eddy-permitting ocean models that are part of coupled AOGCMs (this study and Megann et al, 2014), it is found that the use of an isopycnal mixing parameterisation, based on diffusion, is necessary to obtain a realistic stratification in the ocean. The consequence for our discussion here is that, for the models used in Wolfe et al (2008) and Morrison et al (2013), the temperature change due to eddy advection implicitly contains the temperature change due to isopycnal mixing, while for the model used in this study (HiGEM1.2) the temperature change due to eddy advection and the temperature change due to parameterized isopycnal mixing are diagnosed separately. This makes a direct comparison less than straightforward. Ideally, in future studies of ocean heat uptake processes in high-resolution models the advective and diffusive components of the resolved eddy-induced transports should be diagnosed separately, using the methods by Lee et al (2007) and Eden and Greatbatch (2009). In this context, “diffusive” means “behaving like diffusion if seen from a large-scale perspective”.

Conceptually it is not clear how to separate isopycnal mixing from eddy advection. As Hieronymus and Nycander (2013) point out, isopycnal mixing could be seen as an advective flux like eddy advection. It is just that isopycnal mixing is often parameterized as diffusion, while eddy advection is either resolved or parameterized as advection. This is the main reason why these processes are treated differently in many studies. On the other hand, the eddy advection and the mean advection can be added together and called the residual advection, and it is the residual advection that is actually physically relevant for the tracer transport. In

other words, while it can be argued that the eddy advection should be added to the isopycnal mixing, the same eddy advection can arguably alternatively be added to the mean advection.

To sum up, ocean model studies sometimes use the terms “advective” and “diffusive” arbitrarily. These terms can also depend on the model resolution and/ or the viewpoint of the analysis of the data. This can lead to confusion in model intercomparisons. Eventually the community might want to find a clearer terminology, perhaps by referring to the actual (real ocean) length scales of the processes.

1.2 Previous work

In this section we discuss the literature on ocean heat uptake processes that is relevant in the context of the present study. The reader might want to refer to Table 1, in which the models mentioned below, and the largest terms of their heat budgets, are briefly characterized.

Detailed temperature tendency diagnostics as mentioned above—for temperature change due to advection, the different kinds of diffusion, convection, ice physics, etc.—were used by Gregory (2000) in HadCM2, to analyse vertical heat transports. He found that on a global scale the main balance is between downward advection of warm waters and an upward transport of heat by mixing along isopycnals. This is in opposition to the often assumed advection-diffusion balance with a downward diapycnal heat transport and an upwelling of warm waters (e.g. Munk and Wunsch, 1998).

Using the GFDL ocean model, Gnanadesikan et al (2005) confirmed the result by Gregory (2000) that, in a control run, the main process transporting heat downwards (on the global average) is advection, while the upward heat transport is due to subgridscale processes. These subgridscale processes in Gnanadesikan et al (2005) comprise isopycnal mixing, diapycnal mixing and parameterized eddy advection. Parameterized eddy advection is responsible for the bulk of the upward heat transport, while the sum of isopycnal and diapycnal mixing transport heat downwards. Gnanadesikan et al (2005) also identified convection as an important process for upward heat transport. Wolfe et al (2008) analysed an eddy-resolving and a high-resolution (5.4 km) OGCM (MITgcm and POP), not using a GM type parameterization of eddy-induced transports. In their models, mean advection and vertical diffusion are warming the ocean, while the resolved eddy advection cools it.

Hieronimus and Nycander (2013) used the ocean model NEMO to analyse the vertical heat transport with detailed diagnostics in a long control run. In line with the previous work, they found that mean advection warms the ocean, while the parameterized eddy-induced advection cools it. Parameterized diapycnal diffusion also contributes significantly to the downward heat transport. Hieronimus and Nycander (2013) also looked at the regional features of the isopycnal heat transport and found that it is concentrated in the Southern Ocean and the North Atlantic.

Griffies et al (2015) analysed three versions of the GFDL coupled climate model. Emphasising the role of mesoscale eddies for ocean heat transport, they confirmed that the strongest downward heat transport comes from the mean advection, followed by vertical diffusion. The largest upward heat transport is due to eddy-induced advection (resolved and/or parameterised), followed by mixed layer physics and parameterized sub-mesoscale eddies.

The first study to make use of process-based diagnostics was Manabe et al (1990). They identified the important role of the convection in the Southern Ocean for global ocean heat uptake (OHU). In their control run, deep convection in the high Southern latitudes leads to strong heat loss to the atmosphere. In a 2xCO₂ climate, warming and freshening stabilizes

the water column, reducing convection and thus reducing heat loss, which is equivalent to OHU. Gregory (2000) also identified the dominant role of the Southern Ocean for the global heat budget. In a 1%CO₂ run with HadCM2, the ocean warms because of reduced convection that leads to reduced heat loss from convection and isopycnal diffusion.

While HadCM2 did not have a GM-type parameterization of eddy-induced processes, Huang et al (2003b) analysed ocean heat uptake processes in a coupled model with a GM parameterization. Again in a 1%CO₂ run, but focusing on an idealized Atlantic, they found that convection, parameterized eddy advection and isopycnal diffusion dominate strong OHU in the high latitudes, and that vertical advection is the dominant process for weaker ocean heat uptake in the lower latitudes. These results are in line with the results from Gregory (2000). However, Huang et al (2003b) have only a single diagnostic for the sum of isopycnal diffusion and parameterized eddy advection.

Huang et al (2003a) used an OGCM and its adjoint instead of process-based diagnostics to calculate the sensitivities of ocean heat uptake processes to changes in the surface heat flux. In a 1%CO₂ run, they found (similarly to Gregory (2000)) that deep ocean heat uptake happens mostly in the Southern Ocean and in the North Atlantic, due to suppression of isopycnal cooling and of convective cooling. Banks and Gregory (2006) identified reduced surface heat loss and increased precipitation at high latitudes as the causes for an increased stability of the ocean and for the suppression of convection and upward isopycnal diffusion.

Brierley et al (2010) analysed the ocean heat budget and heat uptake in HadCM3 using almost the same temperature tendency diagnostics that we will use. Globally, the downward (warming) heat transport in the control run is mainly from resolved advection (downwelling) and to a lesser extent from vertical diffusion. The upward (cooling) heat transport is achieved by parameterized eddy advection (GM) and isopycnal mixing, in accordance with earlier results. In their 1%CO₂ run, the heat uptake is mostly due to isopycnal mixing and, in deeper layers, diapycnal mixing.

With a very idealized model, but not using process-based diagnostics, Morrison et al (2013) focused on the roles of the mean and the eddy advection. As in other studies, the mean advection warms the ocean and the (resolved) eddy advection cools it. The residual advection is not analysed. In idealized warming runs, Morrison et al (2013) find (again, in accordance with Gregory (2000)) reduced along-isopycnal mixing (resolved in their model) as the reason for warming. In an increased wind stress run, they find a transient cooling in the ocean interior due to intensified eddy advection in the Southern Ocean.

1.3 Aims of the present study

The focus, and at the same time the novel aspect, of the present study is to analyse in which regions ocean heat uptake is strongest, and what physical processes dominate it in those regions, in an AOGCM with realistic geography and an eddy-permitting ocean component (HiGEM1.2; Shaffrey et al (2009)), including a detailed set of temperature (and salinity) tendency diagnostics. With HiGEM1.2 being a CMIP5-type model, this analysis also contributes to understanding the spread and the biases of projections of thermosteric sea level rise in this class of models.

To analyse the causes for changes in ocean heat uptake we conducted two perturbation runs with HiGEM1.2, one run with a scenario of abrupt CO₂ increase and another run where only the windstress was perturbed. The wind perturbation shows the typical southward shift and intensification of the westerlies in the Southern Hemisphere of model scenarios with increased CO₂. The role of the southward shift of the maximum zonal windstress for ocean

heat uptake in the 20th century was discussed by Cai et al (2010) for the CMIP3 models. They point out the non-local nature of the ocean heat uptake in the mid-latitude Southern Ocean, and the role of increased Ekman transports.

The ocean heat uptake processes we discuss affect the density field in the Southern Ocean, and thus also the flow field, of which the Antarctic Circumpolar Current (ACC) is one of the main features. Wang et al (2011) and Downes and Hogg (2013) discuss the strong role of buoyancy fluxes in determining the response of the ACC in a given GCM to changes in radiative forcing. We will show how the buoyancy fluxes determine the ACC response in HiGEM1.2, and how this relates to the ocean heat uptake processes.

The description of the model, the model runs and the diagnostics are found in sec. 2. The analysis of the ocean heat uptake processes using the temperature tendency diagnostics for the global ocean follows in sec. 3. We then present the regional analysis, with a focus on the Southern Ocean, in sec. 4. The impact of the OHU changes on the ACC are discussed in sec. 5, and the conclusions from the paper's results are drawn in sec. 6.

2 Model and Experiments

HiGEM1.2 is based on the UK MetOffice coupled AOGCM HadGEM1, but has a higher spatial resolution, of 0.83° lat x 1.25° lon (N144) in the atmosphere and $1/3^\circ$ x $1/3^\circ$ with 40 levels in the ocean. With its high resolution HiGEM1.2 is comparatively expensive to run. In the ocean, the resolution is considered to be eddy-permitting. Therefore it was chosen to not use a parameterization of eddy-induced advection. This choice improved the representation of sharp tracer gradients (Shaffrey et al, 2009). The lateral mixing of tracers uses the isopycnal formulation of Griffies et al (1998) with a constant isopycnal diffusivity of $500 \text{ m}^2/\text{s}$. A biharmonic Gent and McWilliams scheme (Roberts and Marshall, 1998) is employed to reduce noise. For the vertical diffusivity a background profile K_{bg} is prescribed as a linear function of depth, and an expression for vertical diffusivity K_{Ri} as a function of the Richardson number (following Peters et al, 1995) is evaluated. At every time step and grid box, the larger of K_{bg} and K_{Ri} is applied in the vertical diffusion scheme. Mixed-layer processes are parameterized by the Kraus-Turner scheme, which does most of the vertical mixing. Convection is parameterized as complete mixing according to Rahmstorf (1993). Present-day boundary conditions were chosen for the control run. In particular, the atmospheric CO_2 concentration was set to 345 ppmv, reflecting conditions in the 1980s.

HiGEM1.2 compares well with observations and other GCMs, as Shaffrey et al (2009) have shown in their detailed description of it. As an example, Fig. 1 displays the globally averaged density profile of HiGEM (green) which is close to observations (black) at most depth levels. In line with most CMIP5 models, HiGEM shows open-ocean deep convection in the Southern Ocean, namely in the Weddell and Ross gyres (Heuzé et al, 2013). This process itself is not realistic, yet it leads to realistic water mass properties in the Southern Ocean. HiGEM compares favourably with most CMIP5 models in this regard (Heuzé et al, 2013). The presence of open-ocean convection goes along with a sea ice cover (mainly the sea ice fraction) that is less than observations in the control run.

2.1 Perturbation runs

The control run (“CTRL”) length is 111 years upon the beginning of the two perturbation runs, which are labeled 4xCO₂ and WIND. These two runs are only twenty years long because of the computationally expensive resolution of HiGEM.

For the 4xCO₂ run, the atmospheric CO₂ content was quadrupled instantaneously to 1380 ppmv. While this is an idealized scenario, it is one of the standard CMIP5 scenarios (although our run is shorter). In particular, Good et al (2011, 2012) showed that the results of a 4xCO₂ run can be scaled to emulate the results from a 1%CO₂ run with only small errors, especially for temperature.

For the wind perturbation run (“WIND”), we diagnosed the monthly mean wind stress fields from the years 11-20 of the 4xCO₂ run, subtracted the same field from the control run and thus calculated a mean seasonal cycle of the wind stress response. Since we are interested in the effect of wind forcing on the Southern Ocean, these response fields were set to zero north of 10° S and linearly tapered to zero in the latitude band between 20° S and 10° S, where the zonal average of the anomalies is close to zero anyway. In the WIND run, the windstress applied to the ocean is the sum of the windstress computed during the run and the prescribed perturbation as function of the time of year. The wind stress perturbation affects only the momentum flux into the ocean, not the bulk formulae for the tracer fluxes.

Fig. 2 shows the zonal wind stress of the control run and the annual mean tapered anomalies. As in many CMIP5 models, the anomalies reflect a poleward shift and a strengthening of the westerlies in the Southern Hemisphere. Equatorwards of the mid-latitude wind stress maximum the meridional gradient of the wind stress intensifies. While this wind stress perturbation is derived from a 4xCO₂ run, a similar wind perturbation would result from a stratospheric ozone depletion (Sigmond et al, 2011).

2.2 Diagnostics of OHU processes

HiGEM has been run with diagnostics for the individual terms of the temperature and salinity equations. These terms, listed in Table 2, comprise the temperature and salinity change due to diffusion (separately in the x, y and z directions), advection, convection, mixed layer physics, ice physics, penetrating solar radiation (for temperature only) and other surface fluxes. In the absence of a GM-type parameterisation, the advection diagnostic naturally contains the (permitted) eddy activity, and therefore represents the effect of the residual advection. (The effect of the biharmonic GM scheme is included in the three diffusion diagnostics.) At each time step the full three-dimensional fields of these terms are diagnosed, and the monthly (and longer-term) means are saved. The original units of the temperature diagnostics are K/s. By multiplying them with the specific heat capacity C_p and a reference density ρ_0 and averaging them over each model layer individually (or over other volumes, as described below) we obtain the unit of W/m³. In this way, the depth profile figures (starting with Fig. 3) show the change in heat content due to each individual process in each layer. The units suggest interpreting the diagnostics as heat convergences. This is found to be more revealing than the vertical integral of this quantity, in the units of a heat flux, since the convergences describe each layer individually.

We have calculated the temporal standard deviation of the individual diagnostics and their sum with the aim of assessing the significance of the anomalies in the perturbation runs. The section of the control run that we analysed is 70 years long, while the perturbation runs are parallel to the first 20 years of the control run section. We calculate a standard deviation

from seven consecutive 10-year means of the control run. A 20-year mean anomaly from the perturbation run on a given level is considered significant if it is outside the 5% to 95% confidence interval (1.65σ) interval around the control run value, and there is an additional factor of $1/\sqrt{2}$ to account for the comparison of a 20-year mean with 10-year means.

2.3 Decomposition of diagnostics

The run-time diagnostics available for HiGEM are a complete set in that their sum gives the total temperature change at any gridpoint. However, they do not resolve all the processes that are relevant. Specifically, this applies to vertical diffusion and advection. The runtime diagnostic for vertical diffusion is the sum of four processes: (1) the vertical component of isopycnal diffusion, (2) the background diapycnal diffusion or the shear-dependent vertical diffusion, (3) vertical diffusion in the mixed layer (following Large et al (1994)) and (4) the vertical component of the biharmonic GM scheme. The shear-dependent mixing and the vertical diffusion in the mixed layer only affect the top 100 m or so and we do not discuss them further, but it is of great interest to decompose the vertical diffusion into its isopycnal and diapycnal component. Introducing them as further runtime diagnostics would have been desirable, but is difficult due to the way vertical diffusion is handled in the HiGEM code. The biharmonic GM scheme is believed to make very small contributions to heat transport on the large scale; we do however not have a separate online diagnostic for it for the same reason.

We use the Partial Ocean Tracer Tendency Emulator (POTTE) to decompose the vertical diffusion diagnostic. POTTE is a set of IDL scripts that allows to infer the fields of some of the tendency diagnostics from the standard output fields temperature, salinity and velocity. It was modeled on the numerical schemes of the AOGCM HadCM3. POTTE can currently emulate the fields of temperature change due to advection, isopycnal diffusion (by spatial components), diapycnal diffusion and advection due to the Gent-McWilliams parameterization of eddy-induced transports. In principle, POTTE can thus provide these diagnostics for any AOGCM or OGCM where only standard output is available. A more detailed description of POTTE is given in Exarchou et al (2015).

By construction POTTE works well for HadCM3. We have tested it for advection and isopycnal and diapycnal diffusion with HiGEM and found that it works well, too, for advection and isopycnal diffusion. For diapycnal diffusion however, we found a marked negative bias in POTTE. Therefore we use POTTE to calculate the temperature change due to the vertical component of isopycnal diffusion. The difference between the runtime diagnostic for vertical diffusion and this POTTE result is then interpreted as the temperature change due to diapycnal diffusion.

In addition to the decomposition of vertical diffusion, it is also desirable to decompose the advection. Since there is no parameterization of mesoscale eddy-induced transports in HiGEM, the advection diagnostic represents the action of the residual advection in the temperature equation. But it is important to know what part of the temperature change is due to the mean advection, and what part due to the eddy advection. Following the decomposition given in sec. 1.1, we use POTTE to calculate the advective temperature change from annual means and interpret this as the mean advective change $\nabla \cdot (\bar{\mathbf{v}}\bar{T})$. The difference between the residual advection and the mean advection is then interpreted as the eddy advective temperature change $\nabla \cdot \overline{\mathbf{v}'T'}$.

3 Global ocean heat uptake processes and their changes

3.1 Global average of the control run

In this section we discuss the globally averaged OHU diagnostics and compare them with other models. A comparison with observational data is highly desirable, but currently not feasible due to lack of a global coverage of process-based observations. OHU is defined as a change in ocean heat content (OHC), where for a given volume V : $OHC = \int_V C_p \rho_0 \theta dV$. Herein, C_p is the specific heat capacity of sea water, ρ_0 a reference density, and θ the potential temperature. (For the calculations, we used a constant value of $\rho_0 C_p = 4.09169 \cdot 10^6 \text{ J m}^{-3} \text{ K}^{-1}$.)

The global integral of all the diagnosed processes vanishes, except for the two components of the surface fluxes that are diagnosed (see Table 2) and an issue with the advection (see sec. 4.5 for details). The incoming penetrating solar (shortwave) radiation warms the ocean, and the other (i.e. longwave) surface fluxes cool it. The sum of these two components is very small, as we will discuss later. The net warming of the 4xCO2 run is due to less cooling.

The vertical structure of the diagnostics, in the control run and the anomalies, is shown in Fig. 3. For this and the following figures, we use a power law scaling for both axes, reflecting the closer spacing of model levels in the upper ocean, and the fact that the diagnostics vary across several orders of magnitude. In the literature, a logarithmic scaling of the axes is often used for such greatly varying variables. This was not applicable here since the diagnostics may have values of either sign or may even equal zero. Hence we have scaled the axes with an exponent of 0.3. Because of this scaling, terms which appear to have fairly modest differences may actually differ by a substantial ratio. To help the reader, the vertical thin dotted lines indicate orders of magnitude. We use this method of presentation so that we can accommodate the whole ocean on a common x-axis and thus facilitate comparison between different depth levels in the same panel. As opposed to the presentation of similar quantities in the literature (e.g. Hieronymus and Nycander (2013)) using linear scales and multiple panels, with our method all the terms can be readily identified and compared at each individual level.

Fig. 3a shows profiles of the diagnostics from the 70 years of control run in thick lines. Thin lines indicate ± 1 standard deviation calculated from seven 10-year means. The upper 100 m are not discussed because the diagnostics are very noisy there, and we are interested in the processes with longer time scales in the deeper ocean. For the sake of clarity we only plot the most relevant diagnostics in Fig. 3. The convection diagnostic, and the sum of the convection diagnostic and the mixed layer physics diagnostic, labelled “VM” for “vertical mixing”, are plotted separately. The other diagnostics (cf. Table 2) are either very small or affect only the surface layers.

From Fig. 3a we see that in the control run of HiGEM1.2 different processes dominate at different depth levels. In the global horizontal average we only see the vertical component of the processes. From below 300 m down to about 3000 m the ocean is warmed by the residual advection (purple curve) and to a lesser extent by diapycnal diffusion (blue). The warming due to residual advection can be decomposed (Fig. 3b): the heating is due to the mean advection (yellow curve), while the eddy advection (dark green) is cooling the ocean. The flattening of the isopycnals associated with eddy advection redistributes the water masses such that, on average, warmer waters are displaced upwards, and colder waters downwards.

The warming by the residual advection is largely balanced by isopycnal diffusion (Fig. 3a, green) below 300 m, and to a lesser extent by vertical mixing (orange). At these depths, ver-

tical mixing is dominated by convection (dotted orange). In short, for depths between 250 m and 3000 m, the main balance for the heat budget of the ocean is between advective warming and isopycnal cooling. HiGEM1.2 is similar to other AOGCMs in this regard, like Gregory (2000) and the model intercomparison by Exarchou et al (2015), of which HiGEM1.2 is part.

The cooling through eddy advection is seen in other eddy-permitting models, e.g. CM2.5 and CM2.6 in Griffies et al (2015), or the idealized model used in Morrison et al (2013). Fig. 1 in Morrison et al (2013) seems to indicate that their residual advection is cooling the ocean, in contrast to our results. In the absence of parameterisations for isopycnal diffusion and for eddy advection, their temperature change due to eddy advection (red curves) contains both these processes. This might be the reason for the cooling dominating. As Fig. 3b shows for our model, the cooling due to isopycnal diffusion and due to eddy advection are of comparable magnitude. Indeed, if we added the isopycnal diagnostic (green) to the residual advection diagnostic (purple), the resulting “super-residual” would be close to zero between 300 m and 3000 m (not shown).

In contrast to Morrison et al (2013), Brierley et al (2010) use an AOGCM (HadCM3) with parameterizations for both isopycnal diffusion and eddy advection. Still, similar to our model, resolved advection and, to a lesser extent, diapycnal diffusion are warming the ocean, while parameterized eddy advection and isopycnal diffusion are cooling it. These results are confirmed for the AOGCMs in Exarchou et al (2015).

Below about 3500 m the balance of processes is different. Here, diapycnal diffusion (blue in Fig. 3a) warms the waters while residual advection and convection cool it. This could be explained by cold Antarctic Bottom Water (AABW) being advected from the Southern Ocean and warming by diffusion from the warmer North Atlantic Deep Water (NADW) above. However, the individual processes are not in equilibrium in HiGEM, as their sum, the total (black) is not zero. This non-zero total mirrors the drift in the HiGEM control run. Nevertheless, the total is at least half an order of magnitude smaller than the dominant processes at almost all levels, and one order of magnitude smaller above 700 m. Note that HiGEM1.2 does not have a parameterization of geothermal heat flux, which can be an important part of the heat budget in the abyss (Hieronymus and Nycander, 2013).

Fig. 3a also shows the standard deviations of the individual diagnostics (thin lines, 1σ intervals). For most diagnostics and at most depth levels, they are so small that they are not visible in the figures. For the total, the 1σ interval straddles the zero line between about 3000 m and 4000 m depth, and above 600 m. This means that the drift is not significantly different from zero in those levels. By contrast, the individual diagnostics are significantly different from zero virtually everywhere.

The balance of OHU processes in HiGEM is rather similar to the widely used OGCM NEMO, as a comparison of our results with those of Hieronymus and Nycander (2013) shows. They analysed a long integration of NEMO 3.2 with a 1° resolution. Like in HiGEM, this is a present-day control run. Their “heat trends” (their Fig. 2) differ from our diagnostics only by a factor of the total surface of each ocean layer. In this NEMO run, residual advection warms the ocean between 600 m and 2500 m, and cools it below. However, at most depth levels the warming from vertical diffusion is stronger than from residual advection. This is unusual for a model with realistic topography. The advective warming is balanced by isopycnal diffusion. This is again a typical feature. Below 3000 m there is a balance between advective cooling and warming from diapycnal diffusion, again much as is HiGEM.

Wolfe et al (2008) analyzed the global vertical heat flux in two models, MITgcm and POP. Comparing POP (having a realistic topography) with HiGEM1.2 (Fig. 3a), we see again some similarities. In both models, mean advection warms the ocean down to a level

between 3500 m (POP) and 4000 m (HiGEM1.2). By contrast, eddy advection cools the ocean down to a level around 3500 m. Both in POP and in HiGEM1.2, the mean and the eddy advection swap signs below that depth. This can be attributed to the northward advection of cold AABW, as in Hieronymus and Nycander (2013). For the next largest term, diapycnal diffusion, there are differences. In HiGEM, the warming effect of vertical diffusion is very small, or even negative, between 1500 m and 3000 m. In POP, vertical diffusion warms the ocean everywhere above 4500 m. As opposed to POP, HiGEM1.2 has also significant convective cooling beyond the winter mixed layer depth, i.e. down to a level of about 2000 m (see further discussion in sec. 4.4).

Overall, we conclude that HiGEM1.2 is a typical AOGCM in terms of its ocean heat uptake processes, with warming from residual advection and isopycnal cooling being the most important processes on the global average. Comparison with other models reveals many differences in detail of the relative importance of the processes.

3.2 Global changes

How does the balance of heat transport processes change in the 4xCO₂ and WIND runs? To address this question we compare the anomalies, which we define as the 20-year averages of the perturbation runs minus the 20-year average of the same period of the control run. We assume that in this way the impact of the residual drift is eliminated. The 4xCO₂ signal of warming (black in Fig. 3c) is bigger than the drift in CTRL (black in Fig. 3a), but it is noteworthy that between 800 m and 2000 m depth they are of the same order of magnitude. This similarity of size is undesirable, and is known to result from insufficient length of spinup runs and imperfect parameterizations of subgridscale heat transport processes. Sen Gupta et al (2012) assessed the ratio of model drift to the 20th century ocean warming. Compared with their results, HiGEM1.2 with its drift to trend ratio of roughly 50% at depth is in line with its parent model HadGEM1 and indeed with all CMIP3 models analyzed in Sen Gupta et al (2012).

The total heat content increases by 950 ZJ (1 ZJ = 10^{21} J) in the 4xCO₂ run, equivalent to a heat flux of 4.1 W/m² through the ocean surface. The depth structure of the 4xCO₂ anomalies is shown in Fig. 3c (note the different scale on the x-axis). There is warming at all depth levels down to the bottom (black curve), even though we analyse only the first twenty years. In the top 1000 m, the warming comes mainly from the vertical mixing processes (orange curve in Fig. 3c). Comparison with Fig. 3a reveals that this warming is actually a reduction of cooling. This, in turn, is connected with a general reduction of mixed layer depth, leading to a reduction in warming due to mixed layer physics (mainly above 500 m, where convection, dotted orange, is small) and convection (below that). Below 1000 m, the ocean is warmed mainly by increased downwelling. There is a small contribution to the warming from reduced isopycnal cooling (compare the green curves in Fig. 3c and Fig. 3a). This could be explained by the vertical structure of the warming, which is stronger at the surface than at depth. As a consequence, the along-isopycnal temperature gradient is reduced, leading to reduced isopycnal cooling.

It is also noteworthy that there is a substantial reduction of diapycnal warming in Fig. 3c. The reason for this is not immediately obvious since the increased vertical temperature gradient should lead to stronger diapycnal warming. Further analysis (not shown) reveals that the decreased diapycnal warming is located in the mid- to high latitudes of both hemispheres. Possibly, our offline calculations of isopycnal diffusion (cf. sec. 2.3) overestimate the reduction of isopycnal cooling in these regions in the presence of the strong isopycnal tilt. Due

to our indirect method of determining diapycnal diffusion (explained in sec. 2.3), this might lead to the apparent reduction of diapycnal warming seen in Fig. 3c.

We have tested the anomalies of the perturbation run for significance, as explained in sec. 2.2. A non-significant anomaly at any level is marked by an “x” in Fig. 3c and Fig. 3d. Given the small standard deviations in the control run, most of the anomalies are actually significant.

The WIND run (Fig. 3d) mainly redistributes heat, and there is only a small net global warming of the ocean of 39 ZJ, or 0.17 W/m^2 . This is remarkable since it could have been expected that the surface fluxes are modified as a result of the effect of the wind stress forcing. The anomaly of the total (black curve) is dominated by changes in the downwelling (purple) as the close proximity of these two curves reveals. The anomaly is significant between 700 m and 3000 m. To some extent, the warming trend between 700 m and 1700 m is counteracted by increased cooling from vertical mixing (orange), i.e. convection. Thus, convection has effects of opposite sign in the two perturbation runs. The reasons for this will be explored in sec 4.4.

Reduced vertical mixing, from convection and mixed layer physics, and increased downwelling are the main warming processes in idealized CO_2 runs in other models, like HadCM3 and MPI-OM (Exarchou et al, 2015). Note, however, that there can be a time dependence. While this study considers the first 20 years of a $4\times\text{CO}_2$ run, Brierley et al (2010) analyse a $1\%\text{CO}_2$ run from HadCM3 after 70 years. In that run, they find that vertical mixing and isopycnal mixing are the dominant warming processes, while advection plays a lesser role. Similarly, in the MITgcm, Huang et al (2003a) found that reduced vertical mixing and reduced isopycnal cooling are the most important processes leading to warming (although their ocean model is forced by relaxation, as opposed to the AOGCMs with heat conservation).

Whether there is a net warming in a WIND-type run seems to depend on details of the applied forcing. Frankcombe et al (2013) found that their eddy-permitting ocean model warms for a merely increased wind speed, while for a poleward shift in the wind speed maximum their ocean cools, in contrast to the present study. Note that Frankcombe et al (2013) modified wind speed, not wind stress. Thus, in their case the surface buoyancy fluxes are affected by the wind forcing too, which might well influence the ocean’s heat budget. The eddy-permitting model by Morrison et al (2013) shows a net warming, too, for an increased wind stress.

4 Regional ocean heat uptake processes

We analyse now the regional differences between $4\times\text{CO}_2$ and WIND in terms of ocean heat uptake, with the aim of understanding where the changes discussed in the previous section actually happen. The global ocean heat uptake pattern (Fig. 4) is defined as the difference in the ocean heat content, averaged over 20 years, between the perturbation runs and the control run, expressed as the vertical column integral in GJ/m^2 . Fig. 4 shows that in the Southern Ocean there is a band of large OHU in the mid-latitudes (around 40° S to 50° S) in both runs. The $4\times\text{CO}_2$ run (Fig. 4a) shows regions with large heat uptake in the North Atlantic, in the Arctic and to a lesser extent in the North Pacific. With the exception of some small signal in the North Atlantic, this OHU in the Northern Hemisphere does not happen in the WIND run (Fig. 4b). From comparing Figs. 4a) and b) we can infer that the OHU maxima in the mid-latitude Southern Ocean are mainly wind-driven, since they appear in both the perturbation runs. By contrast, we expect the ocean heat uptake in the high-latitude

Southern Ocean to be driven by the surface fluxes, since it does not appear in the WIND run. The regional pattern of OHU in HiGEM is a typical representative of the CMIP5 models, as a comparison of Fig. 4a) with Kuhlbrodt and Gregory (2012) (their Fig.2, supplement) reveals.

For discussing the regional features, we define a few latitude belts that we will discuss in turn:

- Northern Extratropics (“NEx”): 30° N to 90° N
- Tropics: 30° S to 30° N
- Southern Hemisphere, mid-latitudes (“SHeMi”): 60° S to 30° S
- Southern Hemisphere, high latitudes (“SHeHi”): 90° S to 60° S

Furthermore, there are some specific regions that we will refer to, which are outlined by green rectangles in Fig. 4:

- Southwest Indian Ocean (“In”): 20° E to 75° E and 43° S to 37° S
- Argentine Basin (“Ar”): 58° W to 0° E and 50° S to 35° S
- Weddell Gyre (“W”): 55° W to 0° E and 75° S to 62° S
- Ross Gyre (“R”): 178° W to 138° W and 75° S to 65° S
- Drake Passage (“DP”): 69.33° W to 68° W and 68° S to 55° S

The profiles of the advection diagnostic have to be interpreted differently now since the volumes over which the advective heating is averaged have lateral boundaries. Thus, as opposed to the global averages, there will be a lateral advective heat transport, which cannot be separately diagnosed. The other diagnostics (diapycnal mixing, the vertical component of isopycnal mixing, convection and mixed layer physics) are vertical by definition, so their interpretation does not change.

4.1 Northern Extratropics

In the Northern Extratropics, the heat budget is dominated in the control run by advective warming down to about 2000 m (purple line in Fig. 5a). This is balanced mostly by vertical mixing (orange line), which is mostly convection (dotted orange) below ~ 700 m, and to some extent by isopycnal cooling (green line), especially at depths between 300 m and 700 m. Diapycnal mixing plays a minor role in warming the ocean. Below 2000 m, the heating/cooling rates are very small. The total warming rate is not significantly different from zero in the top 1000 m, where the magnitude of the heating/cooling processes is large. There is a slight positive drift below 1000 m.

As is visible in Fig. 4a, the Northern Extratropics warm up significantly in $4\times\text{CO}_2$. Fig. 5c shows that this is largely due to decreased warming by mixed layer physics since the total warming (black) is almost fully explained by the positive anomaly of vertical mixing (orange), with the convection anomaly (dotted orange) small or negative above ~ 700 m. Reduced isopycnal cooling plays a minor role, and there is some compensating reduced diapycnal warming (blue). In WIND there is no significant OHU in the Northern Hemisphere.

In the Arctic Ocean proper (not shown) the warming is actually mostly advective, and reduced convection is less important for the warming. The mixed layer depth is very small already in the control run, and is further diminished by a strong freshening in the surface layer (from sea ice melt). This suggests that the warming in the Arctic is due to lateral advection from the North Atlantic.

4.2 Tropics

In the Tropics region, the heat budget in the control run is a balance between diapycnal downward heat flux (blue line in Fig. 5b) and an upward and/or lateral advective heat transport (purple) in the top 1000 m. Thus, we find here the classical advection-diffusion balance (e.g. Munk and Wunsch, 1998). Contrary to their assumption, neither is this balance found in other regions of the world ocean, nor is the global heat budget dominated by the advection-diffusion balance. Rather, the global budget is dominated by downward advective heat transport and upward isopycnal diffusion of heat (Fig. 3a). Our results, obtained from a fully coupled AOGCM, confirm earlier results from an idealized ocean-only model (Morrison et al, 2013).

In the 4xCO₂ run (Fig. 5d), we find a significant warming between 200 m and 500 m depth, caused advectively, i.e. either by a reduced upwelling of cold waters or by lateral advection. By contrast, in WIND there is an advective cooling, in the same depth range.

4.3 Southern Hemisphere mid-latitudes

In the Southern Hemisphere mid-latitudes, the heat budget is dominated by downwelling and lateral advection of warm waters, and cooling through isopycnal mixing, on a large range of depth levels, from 300 m down to about 3500 m (Fig. 6). Isopycnal mixing is also the prevailing cooling mechanism on the global average (see Fig. 3). The Southern Hemisphere mid-latitudes region is of interest because it contains two regions of strong OHU, in the Argentine Basin and the Southwest Indian Ocean. Notably, this strong OHU occurs in both 4xCO₂ and WIND. Fig. 6b and Fig. 6c reveal that the depth structure of the warming is indeed similar. There is a clear signal of warming in the upper 2000 m or so (black lines). From 400 m downwards, this warming is advectively caused (purple), i.e. downwelling and/or lateral advection are enhanced. Above 400 m there is a large contribution from decreased cooling by vertical mixing (orange, mostly mixed layer physics), more so in 4xCO₂. A detailed analysis (not shown) of the two regions with maximal OHU shows that the windstress changes in both 4xCO₂ and WIND lead to stronger wind stress curl and stronger Ekman pumping. Cai et al (2010) diagnose nonlocal warming from surface fluxes south of 50° S, along with the increased Ekman pumping, as the causes for the warming in the Southern Hemisphere mid-latitudes in the CMIP3 models.

4.4 Southern Hemisphere high-latitudes

Fig. 7a shows that in the Southern Hemisphere high-latitude region, in the control run, the ocean heat transport processes have a larger magnitude at depth than in the Southern Hemisphere mid-latitudes. This is true for advection, but even more so for convection (dotted orange line in Fig. 7a). In this region, convection does nearly all of the vertical mixing below ~600 m, as revealed by the close proximity of the dotted orange line (convection) to the solid orange line (convection + mixed layer physics). In the Southern Hemisphere high-latitude region, we find two smaller region of interest, the Ross Gyre and the Weddell Gyre. In these regions the mixed layer is very deep, suggesting ongoing deep-water formation. As Fig. 4 shows, the response in 4xCO₂ and WIND is different here. The deep-water formation regions warm in 4xCO₂, but cool in WIND. Fig. 7b and Fig. 7c show why. In 4xCO₂, in the whole Southern Hemisphere high-latitude region, the warming (black line) reaches

much deeper than in the mid-latitudes, and this is due to reduced convection (dotted orange line), whereas in the mid-latitudes, it is advection that is responsible for the warming. In the WIND run, we find a significant cooling at depth (below 1000 m), which is due to increased convective activity. In the eddy-permitting ocean-sea ice model by Frankcombe et al (2013) a similar effect is seen (in their W_{4S} experiment), whereas in the idealized eddy-permitting model by Morrison et al (2013) the mid-depth cooling in the enhanced wind stress experiment is attributed to increased eddy-induced cooling. We speculate that the dominance of the heat fluxes due to vertical mixing is a feature of models with realistic topography, explicitly modeled sea ice and a nonlinear equation of state. (In the high-latitude Southern Ocean the dependence of density on temperature is very weak.) In short, in WIND the vertical mixing is decreased in the Southern Hemisphere mid-latitudes—in the depth range 200–500 m relevant for that region—but increased in the high latitudes. The heat loss in the high latitudes (and in the tropics) almost compensates the heat gain in the mid-latitudes, such that the net global OHU in WIND is very small.

We explore the different response of the deep-water formation sites in 4xCO₂ and WIND in more detail. In 4xCO₂, there is an increase in maximum sea ice cover in the coastal regions, and less sea ice cover away from the coasts (Fig. 8b), while in WIND the sea ice cover decreases almost everywhere (Fig. 8c). (The Ross Gyre is an exception, with increased sea ice cover in both runs.) What we find is that in 4xCO₂ there is a strong freshening in the coastal surface layer, which is not seen in WIND. The source of this freshwater is increased precipitation in 4xCO₂. This freshwater layer increases the vertical density gradient in the surface layer, thus stopping deep water formation. In the WIND run, by contrast, the reduced sea ice cover leads to enhanced deep water formation.

The Ross Gyre is a special case because the deep water formation is exceptionally deep there. In the control run, convection is cooling the ocean at almost all levels. In 4xCO₂, the warming is of a similar magnitude at all depth levels down to the bottom (not shown), i.e. as large in the abyss as at mid-depth. The anomalies in 4xCO₂ are thus particularly large. Therefore, the cessation of convection in 4xCO₂ leads to a surface cooling, which does not happen in the other regions in the high-latitude Southern Ocean. It is this cooling that enables the sea-ice cover to expand in the Ross Gyre. Another factor in favour of a build-up of ice cover in the Ross Gyre might be the wind forcing. As Fig. 2b shows, the anomalous wind stress is smaller in the Ross Gyre region than at many other longitudes. We speculate that the weaker wind stress anomaly in the Ross Gyre favours build-up of sea-ice.

A similar mechanism of decreased convection was found in a 1%CO₂ run with CCSM3, one of the CMIP3 models (Kirkman IV and Bitz, 2011). They attribute the stabilization of the ocean south of 60° S mainly to a surface freshening, which however comes from a reduction in sea ice growth near Antarctica, a reduced northward sea ice export and more sea-ice melt further south, in contrast to the precipitation changes in HiGEM1.2.

4.5 Comparison of the regions

A comparative perspective on the ocean heat uptake processes in the regions discussed above is given in Fig. 9. Here, the dominant terms in the entire volume of the individual regions are plotted. The largest terms are advection and the surface fluxes (the two components described in sec. 3.1 added together). The other diagnostics (e.g. the horizontal components of the diffusion processes) are mostly small; for some regions there is a discernible response in the ice physics, which is however always smaller than the response in the total surface fluxes and the advection. Therefore we have omitted it here, along with the rest of the diag-

nostics. Finally, the total sum of the diagnostics is plotted in Fig. 9 (red bars). This contains all diagnostics, with no omissions. In an integral over the whole water column, as in Fig. 9, the vertical mixing (VM) and the vertical diffusion diagnostics vanish by construction.

For every model run and every region, the magnitude of the three components (surface fluxes, advection and total heating rate) is plotted in Fig. 9a. In each triplet, the first bar is for the control run, the second bar is for the 4xCO₂ run (darker hue), and the third bar is for the WIND run (lighter hue). Fig. 9b shows the anomalies of the perturbation runs. Therefore there are only two bars in each group: the first bar (darker hue) displays the 4xCO₂ anomaly for each component and region, and the second bar (lighter hue) displays the WIND anomaly, again for each component and region. For instance, in accordance with Fig. 4 we see that the Weddell Sea gyre warms in the 4xCO₂ run (larger net heating rate, dark red bar), but cools in the WIND run (the light red bar indicates a negative heating rate). By contrast, the mid-latitude Southern Ocean (“SHeMi”) warms in both the 4xCO₂ and the WIND run, as indicated by the dark red and the light red bar both being positive, while in the control run there is a net cooling, indicated by the negative first red bar in Fig. 9a.

As is to be expected, the high-latitude regions (NEx, SHeHi, Wed and Ros) have a negative surface heat flux (Fig. 9a), while the mid- and low latitude regions (Tropics and SHeMi) gain heat from the surface fluxes. The 4xCO₂ warming (the dark red bars) comes from a reduction of surface cooling in the high-latitude regions (dark blue bars), which is counteracted by a reduced advective warming (dark green bars). The high-latitude regions on the Southern Hemisphere are cooling in WIND (negative light red bars), which is mostly due to a reduced advective warming (light green bars).

The Southern Hemisphere mid-latitudes are different, because they are warming in WIND, and because this warming is due to increased advective warming. By contrast, the warming in 4xCO₂ in this region is mostly due to increased surface warming, with some support from advection. This contrast is remarkable because the depth structure of the warming in these two cases is very similar (Fig. 6).

An analysis of the volume-integrated heating rates, as opposed to the volume-averaged heating rates in Fig. 9, reveals the relative contribution of the individual regions to the global net warming. These relative contributions are: 26% for NEx, 32% for Trop, 35% for SHeMi, 6% for SHeHi and 1% each for Wed and Ros. In other words, the strongest contribution to the global net warming comes from the Southern Hemisphere mid- and high latitudes (41% altogether), followed by the Tropics and eventually the Northern Extratropics.

Finally, the global ocean shows a warming from surface fluxes even in the control run—this is what ultimately causes the drift. There is also a very small advective cooling in all three runs. This stems from the imperfect way the free-surface boundary condition is formulated in the model; it is not caused by the diagnostics.

5 ACC response

The Antarctic Circumpolar Current (ACC) is the strongest current in the world ocean. At Drake Passage, its transport is currently estimated to be 153 ± 5 Sv (Mazloff et al, 2010). It is intimately linked with the global meridional overturning circulation (MOC). The ACC and the MOC are the dominant features of the large-scale circulation in the Southern Ocean. In climate models the strength of the ACC is not well constrained: the model mean from the CMIP5 models (Meijers et al, 2012) is 155 ± 51 Sv. Thus the ACC strength in Drake Passage in HiGEM1.2, 190 Sv in CTRL, is within the range of the CMIP5 models.

Here we will analyse how the ACC is changing in the perturbation runs, and how this relates to the ocean heat uptake processes. Since the ACC is driven by a combination of wind stress and buoyancy fluxes (Marshall and Radko, 2003), we expect both these forcings to influence the ACC strength. Fig. 10 shows the development of the ACC—measured as the volume transport through the Drake Passage—in the 70 years of CTRL (black line) and in the perturbation runs (red: 4xCO₂, blue: WIND). In the first 20 years of the control run there is a slight downward trend (dashed) of -2.2 ± 0.7 Sv/decade, after which the ACC transport stabilizes around 184 Sv. In 4xCO₂ there is a strong downward trend (-9.1 ± 0.9 Sv/decade), bringing the ACC transport to 175 Sv after 20 years. This weakening of the ACC under a scenario of increased CO₂ forcing is shown by the majority of the CMIP5 models (Meijers et al, 2012).

In contrast to 4xCO₂, in WIND the ACC transport strengthens to 200 Sv after 20 years, with an upward trend of 4.7 ± 0.9 Sv/decade. This is remarkable because in other AOGCMs with an eddy-permitting grid resolution in the ocean component (e.g. GFDL CM2.4, Farneti et al, 2010) the ACC strength does not increase under a scenario with increased wind stress. This might seem surprising at first since the nominal resolutions of HiGEM and CM2.4 are similar, namely $1/3^\circ$ and $1/4^\circ$. However, while in HiGEM the grid spacing is constant in latitude and longitude everywhere, in CM2.4 the resolution increases with latitude like in a Mercator grid, such that the actual resolution at 60° S is about $1/8^\circ$. This resolution allows the dynamic response of the eddy field that Farneti et al (2010) describe. By contrast, in the mid- to high-latitudes the resolution of HiGEM only permits a flow field with small-scale standing eddies, but little temporal variability.

A reduced ACC transport in climate change simulations has been explained by the narrowing of the ACC in combination with processes that affect the baroclinic structure of the ocean and specifically the tilt of the isopycnal surfaces (Wang et al, 2011). We discuss these two causes in turn. The narrowing is defined as a decrease in the area occupied by the ACC. In order to understand the diverging responses of the ACC in the two perturbation runs, we analyse the ACC area, defined as the area between the northernmost and southernmost streamlines that go through Drake Passage, as shown in Fig. 11. In CTRL, this area is about 29,200,000 km². In WIND, the ACC area increases by 7%, while in 4xCO₂ it is reduced by 5%. This reduction is mostly due to an enlargement of the subpolar gyre in the Weddell Sea and, in an overlapping longitude range, a poleward shift of the Agulhas Current. The narrowing and weakening of the ACC occurs also in the 2%CO₂ run of HiGEM1.1 (Graham et al, 2012). Here, the DPT is reduced from 176 Sv to 162 Sv, and the narrowing occurs both on the northern flank of the ACC, mainly in the Indian Ocean sector, and on the southern flank, mainly in the regions of the Weddell Gyre and the Bellingshausen Sea. These results are very similar to what we find in HiGEM1.2.

To explain why this narrowing occurs we need to understand why the Weddell Gyre is extending. From the barotropic streamfunction (Fig. 11) we see that the Weddell Gyre is also strengthening, from about 50 Sv in CTRL to 70 Sv in 4xCO₂. The surface density is decreasing in this area, but not in a way that would be particularly strong in comparison with other latitude ranges. Therefore, this cannot explain why the Weddell Gyre expands and strengthens, while the Ross Gyre does not do that. It is more revealing to look at the wind stress changes in more detail. Fig. 2b shows that the wind stress anomalies in the region around 0° E, where the Weddell Gyre spins up, are clearly stronger than in the Ross Gyre region. It is also in this longitude range (between 0° E and 90° E) where the equatorward contraction of the ACC is strongest (Fig. 11).

Next we turn to assess the changes in the baroclinic structure. Since these vary considerably with latitude and longitude, and since we are interested in the transport through the

Drake Passage, we analyse the baroclinic structure and its changes in the Drake Passage region (DP in Fig. 4). As we would expect, the isopycnal surfaces (potential density σ_2) are strongly tilted across DP (colour shading Fig. 12). In line with the changes in DP transport depicted in Fig. 10, the isopycnals flatten in 4xCO₂ (Fig. 12a) and steepen in WIND (Fig. 12b). The density changes in 4xCO₂ (denser at the northern end of DP, lighter in the subsurface core section) can be attributed mainly to temperature changes (cooling/warming; not shown). The density changes in WIND—lighter in a wedge-shaped region from the surface down to ~ 500 m at the southern end of DP sloping down to ~ 1000 m at the northern end—are, by contrast, mainly caused by freshening. The cooling, in 4xCO₂, at the northern end of DP is mainly caused by a reduction in convection (around ~ 400 m), in mixed layer processes (above that) and in vertical diffusion (below ~ 400 m). The subsurface warming in 4xCO₂ comes from the reduced convection, too, but more so from advection, which will be lateral advection in all likelihood, given the presence of the strong current. The freshening in WIND can be largely attributed to advection as well, and to some extent to an increased convective activity. The changes in convective and mixed layer activity in both perturbation runs are in accordance with the changes in the mid-latitude Southern Ocean in general (sec. 4.3).

We had attributed the different response of vertical mixing in the both perturbation runs to the different freshwater fluxes in sec. 4.4. Thus, we can conclude that the precipitation increase in 4xCO₂ is crucial for explaining both the different response of the ACC and the differences in OHU in 4xCO₂ and WIND. The freshening triggers a reduction of convection in 4xCO₂, leading to net OHU in the full water column, with cooling in the top layer and warming below. These changes in temperature and salinity affect the baroclinic structure in opposite ways in 4xCO₂ and WIND.

6 Conclusions

The purpose of this paper is to analyse the ocean heat uptake processes globally and regionally using detailed diagnostics of the temperature tendencies in HiGEM1.2, an AOGCM with realistic geography and an eddy-permitting ocean component. The novelty is the focus on which ocean heat uptake processes are dominating in which regions.

For the global heat budget, the Southern Ocean is the most important region, and the dominant balance is between downward advective transport and upward isopycnal diffusion, as found in previous model studies, while in the upper tropical ocean we find the traditionally assumed diapycnal diffusion/upwelling balance. In the Northern Extratropics, convection and mixed layer physics are the most important cooling process, balancing downward advection. The decomposition of the global downwelling shows that the eddy advection cools the ocean, as in several other models. The cooling from eddy advection and from isopycnal diffusion are of the same order of magnitude. It can be argued that they could be added together since they can be both seen as diffusive processes on isopycnals, and combined with mean advection to give a new “super-residual” advection.

The advective (that is, due to downwelling and/or lateral advection) warming goes deepest in the high-latitude regions of the Southern Hemisphere. As a consequence, the changes in the perturbation runs have their deepest extent in this region too. In the Ross Gyre, the warming in 4xCO₂ extends down to the bottom.

The 4xCO₂ and WIND runs give quite different results for the high-latitude Southern Ocean area. The ocean heat uptake there in 4xCO₂ is explained by reduced convection, triggered by freshwater input from precipitation. In WIND, there is increased convective

activity, and therefore a heat loss from the ocean. Due to the increased precipitation and the ensuing freshwater lid, the same wind stress forcing cannot trigger more convection in the 4xCO₂ run.

Seen as a whole, the warming in the 4xCO₂ run is due to changes in convection and mixed layer physics in the high latitudes on both hemispheres, and due to advection in the Southern Hemisphere mid-latitudes. In the WIND run, the windstress forcing in the Southern Hemisphere redistributes the heat content, but only leads to a very small global OHU.

The interplay of freshwater and wind forcing also explains why the ACC is strengthening in WIND while it weakens in 4xCO₂. The diminishing ACC in 4xCO₂ is due to a narrowing of the ACC, caused by a wind-driven expansion of the Weddell Gyre, and due to a flattening of the isopycnals caused by the suppression of vertical mixing. Conversely, the enhanced vertical mixing in WIND leads to a steepening of the isopycnals in the Drake Passage and thus to a stronger transport across it.

Comparison of our results with other models reveals many differences in detail of the relative importance of the processes. These differences call for a further analysis, in order to relate them to the models' formulation and control states. For this purpose, it would be very helpful to have accurate online diagnostics of all relevant ocean heat uptake processes. This would allow for more accuracy and detail in future model intercomparison studies.

A caveat in this study is that the modeled open-ocean deep-water formation in the Southern Ocean is unrealistic, like in all AOGCMs of a comparable resolution. A similar study in a high-resolution AOGCM would be very interesting if it had a better representation of the on-shelf deep-water formation processes in the Southern Ocean. Still, we believe that such a model would confirm the importance of regional ocean heat uptake processes for the global heat budget and the relevance of salinity changes for some regional changes in ocean heat uptake.

Acknowledgements We are grateful to Dave Stevens and Ian Stevens for help and support with running HiGEM1.2 and investigating the model code. The comments of Steve Griffies and two anonymous reviewers have led to important clarifications in the paper. The research leading to the results presented here has received funding from the European Research Council under the European Community's Seventh Framework Programme (FP7/2007-2013), ERC grant agreement number 247220, project "Seachange", and from the National Centre for Atmospheric Science (NCAS) Climate Programme.

Table 1: Overview of the ocean models whose results are discussed in sec. 1.2. The columns, from left to right, give the study we are citing, the horizontal resolution of the ocean model, the number of vertical levels, whether it is a coupled atmosphere-ocean model, whether the GM parameterization has been used, the isopycnal diffusion coefficient (if a parameterization for isopycnal diffusion was used at all), and—in the last column—the largest terms of either sign (warming \oplus or cooling \ominus) of the global heat budget between approximately 200 m and 1500 m depth. Here, the results for the full budget of the control run (**CTL**) are given in upright typeface, and the results for the *anomalous* fluxes in global warming scenarios (CO_2) are given in *italics*. These global warming scenarios are mostly idealized. The abbreviations in the last column are “adv” for resolved advection, “dia” for diapycnal mixing, “iso” for isopycnal mixing, “VM” for vertical mixing (the sum of convection [“conv”] and mixed-layer physics), “mean” for mean advection, “edd” for resolved eddy advection and “GM” for parameterized eddy advection. If two processes are written together with a plus (e.g. “(GM+iso)”) then they have not been diagnosed separately.

Study	Resolution	Le- vels	Coup- led	GM used	Isopyc. diff. coefficient	Largest budget terms glob- ally ($\sim 200 - 1500$ m)
Banks and Gregory 2006	1.25°	20	yes	yes	1000 m ² /s	CO_2 : <i>adv</i> \oplus , <i>VM</i> \oplus
Brierley et al. 2010	1.25°	20	yes	yes	1000 m ² /s	CTL : <i>adv</i> \oplus , <i>GM</i> \ominus CO_2 : <i>iso</i> \oplus , <i>conv</i> \oplus
Gnanadesikan et al. 2005	4.5°lat \times 3.75°lon	24	no	yes	1000 m ² /s	CTL : <i>adv</i> \oplus , <i>GM</i> \ominus
Gregory 2000	2.5°lat \times 3.75°lon	20	yes	no	400– 2000 m ² /s	CTL : <i>adv</i> \oplus , (<i>iso</i> + <i>dia</i>) \ominus CO_2 : <i>adv</i> \oplus , (<i>iso</i> + <i>dia</i>) \oplus
Griffies et al. 2015: CM2-1deg	1°	50	yes	yes	600 m ² /s	CTL : <i>adv</i> \oplus , <i>GM</i> \ominus
Griffies et al. 2015: CM2.5	0.25°	50	yes	no	none	CTL : <i>mean</i> \oplus , <i>edd</i> \ominus
Griffies et al. 2015: CM2.6	0.1°	50	yes	no	none	CTL : <i>mean</i> \oplus , <i>edd</i> \ominus
Hieronimus and Nycander 2013	1°	46	no	yes	1000 m ² /s	CTL : <i>adv</i> \oplus , <i>GM</i> \ominus
Huang et al. 2003a	4°	15	yes	yes	1000 m ² /s	CO_2 : <i>conv</i> \oplus , (<i>GM</i> + <i>iso</i>) \oplus
Huang et al. 2003b	4°	15	no	yes	1000 m ² /s	CO_2 : <i>conv</i> \oplus , (<i>GM</i> + <i>iso</i>) \oplus (below 700 m)
Manabe et al. 1990	4.5°lat \times 3.75°lon	12	yes	no	none	CTL : <i>adv</i> \oplus , <i>conv</i> \ominus CO_2 : <i>conv</i> \oplus , <i>adv</i> \ominus
Morrison et al. 2010	0.25°	36	no	no	none	CTL : <i>mean</i> \oplus , <i>edd</i> \ominus CO_2 : <i>edd</i> \oplus
Wolfe et al. 2008: MITgcm	5.4 km	20	no	no	none	CTL : <i>dia</i> \oplus , <i>edd</i> \ominus
Wolfe et al. 2008: POP	0.1°	40	no	no	none	CTL : <i>mean</i> \oplus , <i>edd</i> \ominus
This study	0.33°	40	yes	no	500 m ² /s	CTL : <i>adv</i> \oplus , <i>iso</i> \ominus CO_2 : <i>VM</i> \oplus , <i>adv</i> \oplus

Table 2: Terms of the tracer transport equations as diagnosed on runtime in HiGEM1.2. Z-diffusion and advection are further decomposed, using POTTE, into the components after the colon.

x-diffusion	ice physics
y-diffusion	mixed layer physics
z-diffusion: isopycnal, diapycnal	convection
penetrating solar radiation	advection: mean, eddy-induced
other surface fluxes	

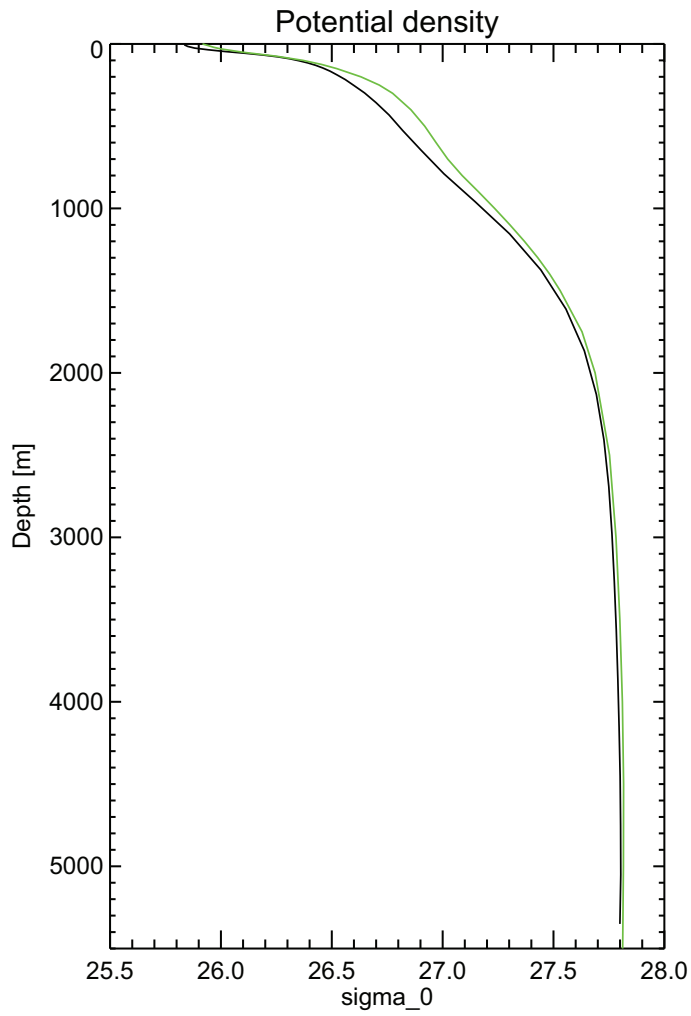


Fig. 1: Globally averaged density profile from the World Ocean Atlas 2009 (black, *Locarnini et al., 2010*) and the HiGEM control run (green, 20-year average).

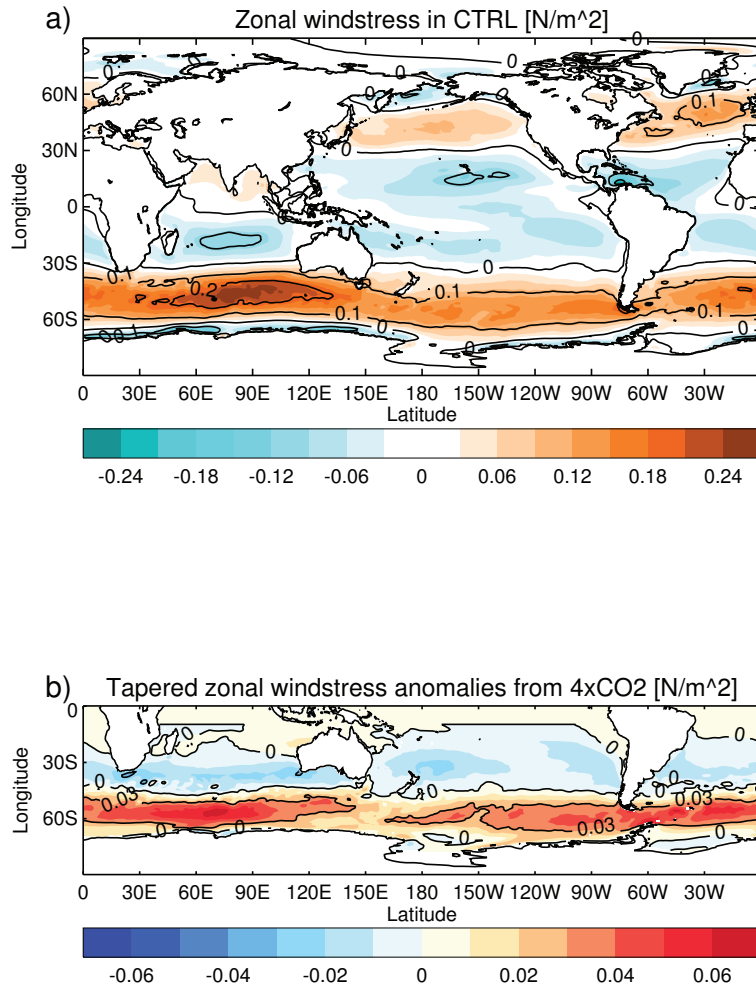


Fig. 2: (a) Zonal windstress in the control run, averaged over model years 2100 to 2110. (b) Anomalies of the zonal wind stress in the Southern Hemisphere in the 4xCO2 run averaged over the same period and tapered north of 20° S as described in the main text. The intensification of the westerlies is strongest in the Indian Ocean sector and weakest in the southwest Pacific sector of the Southern Ocean.

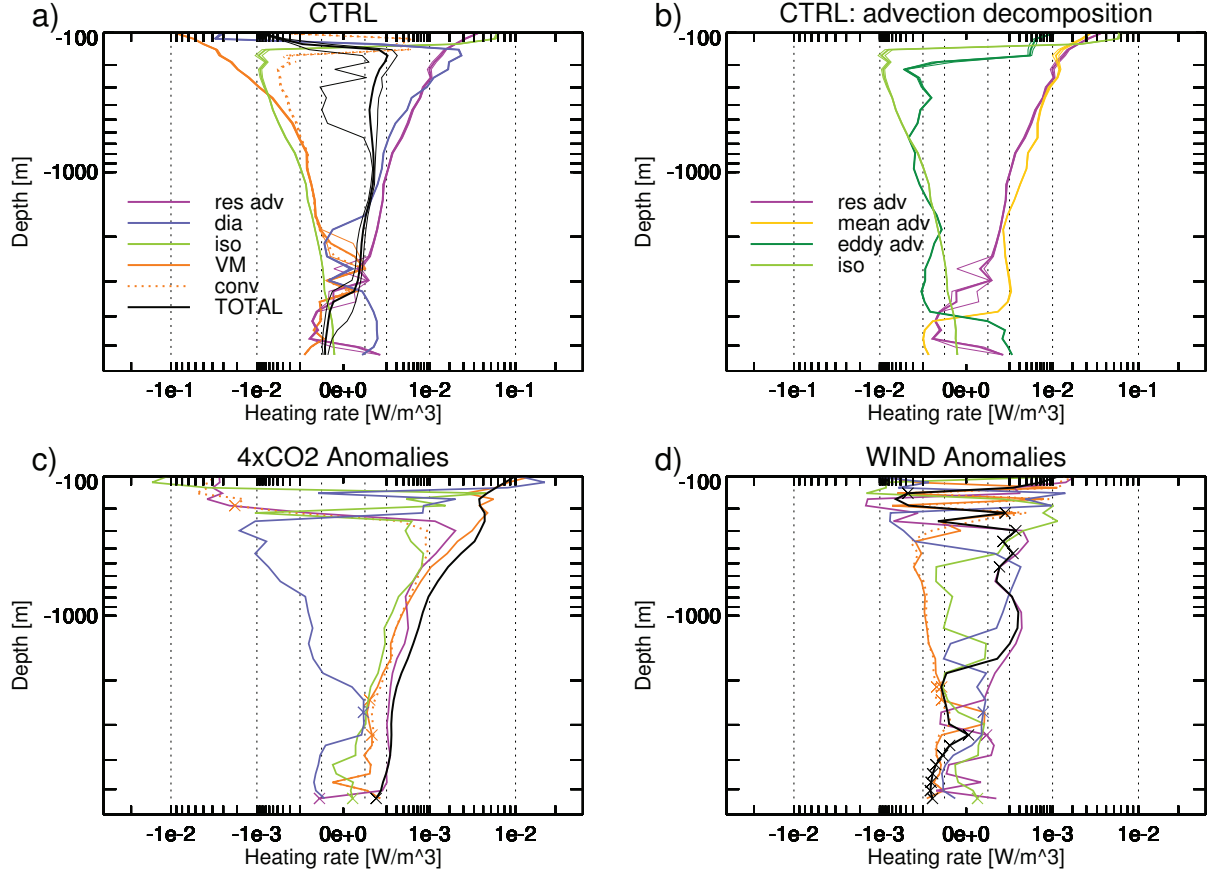


Fig. 3: The temperature tendency diagnostics as a function of depth in HiGEM1.2. Bold lines show a 70-year average from the control run and 20-year averages from the perturbation runs. The thin lines indicate a ± 1 standard deviation interval for the control run (CTRL). They are shown for the components as well as the total, but are hardly discernible since the standard deviation is relatively small in all of the cases. Both axes are stretched according to a power law to visualize both the large values in the mixed layer and the small values at depth. Dotted black vertical lines mark orders of magnitudes. (a) CTRL, (b) decomposition of advective temperature change in CTRL, (c) 4xCO₂ minus CTRL, (d) WIND minus CTRL. Note the differing scale on the x-axis for panels (c) and (d). The individual processes are described in section 2.2. The abbreviations in the legend are “res adv” for residual advection, “dia” for diapycnal mixing, “iso” for isopycnal mixing, “VM” for vertical mixing (the sum of convection, “conv”, and mixed-layer physics), “mean adv” for mean advection and “eddy adv” for eddy advection. The crosses denote non-significant data points as explained in the text.

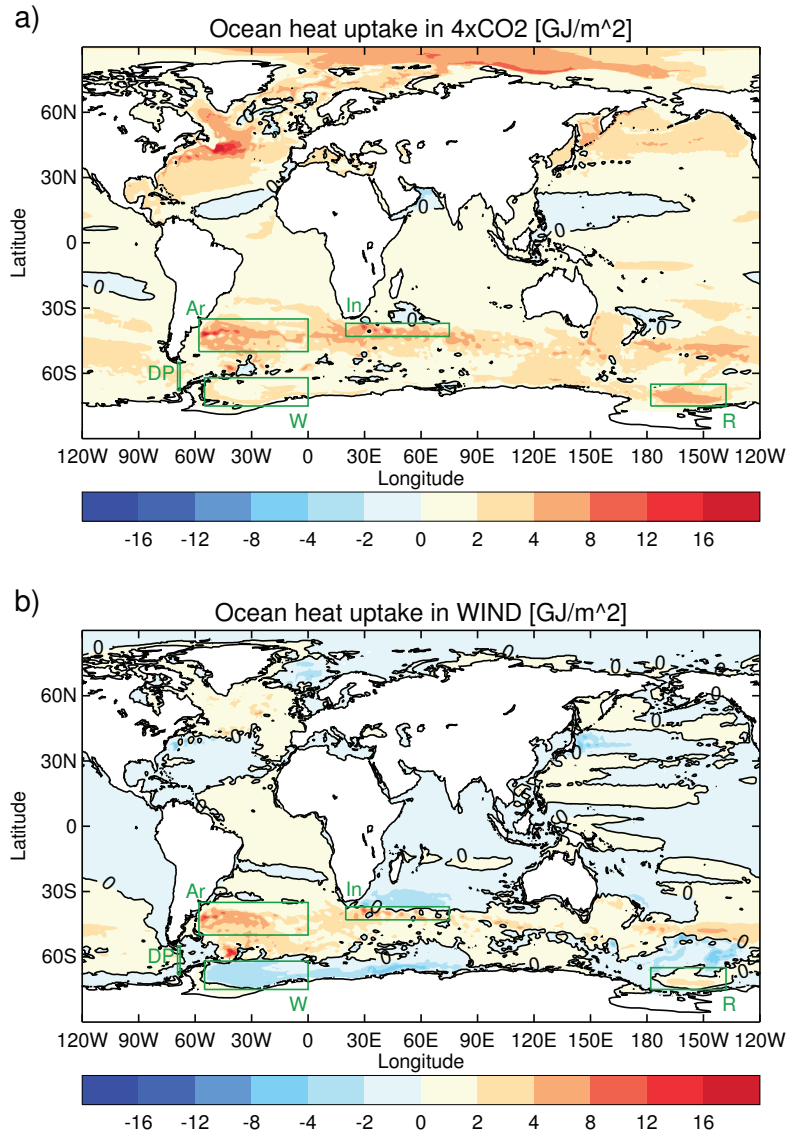


Fig. 4: Ocean heat uptake on the global average and averaged over the 20 years of the perturbation runs (a) 4xCO₂ and (b) WIND. The intervals of the colour scale are not constant. Green rectangles, marked with letters, show the regions of special interest. These are, in the Southern Hemisphere, from left to right: Drake Passage (DP), Argentine Basin (Ar), Weddell Gyre (W), Southwest Indian Ocean (In) and Ross Gyre (R).

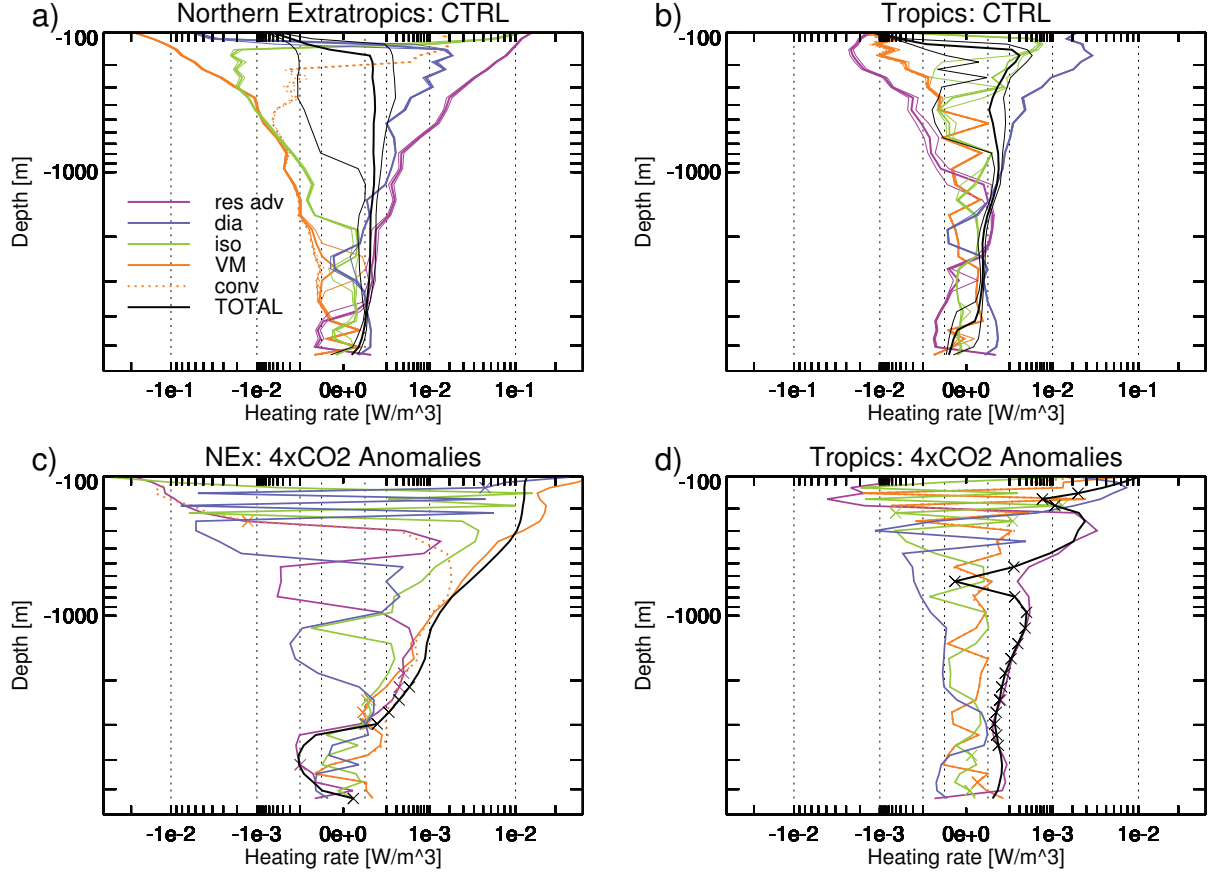


Fig. 5: Horizontally averaged temperature tendency diagnostics for (a) the control run in the Northern Extratropics region, (b) the control runs in the Tropics region, and the 4xCO₂ anomalies in (c) the Northern Extratropics and (d) the Tropics region. Both axes are stretched according to a power law to visualize both the large values in the mixed layer and the small values at depth. The dotted vertical lines denote orders of magnitude. Note the varying scales on the x-axis. Bold lines give the actual values, and thin lines (in the control run plots) indicate a ± 1 standard deviation interval. The standard deviations are shown for the components as well as the total, but are hardly discernible since the standard deviation is relatively small in all of the cases. See sec. 4 and Fig. 4 for the definition of the regions. For the abbreviations in the legend, see caption of Fig.3. The crosses denote non-significant data points as explained in the text.

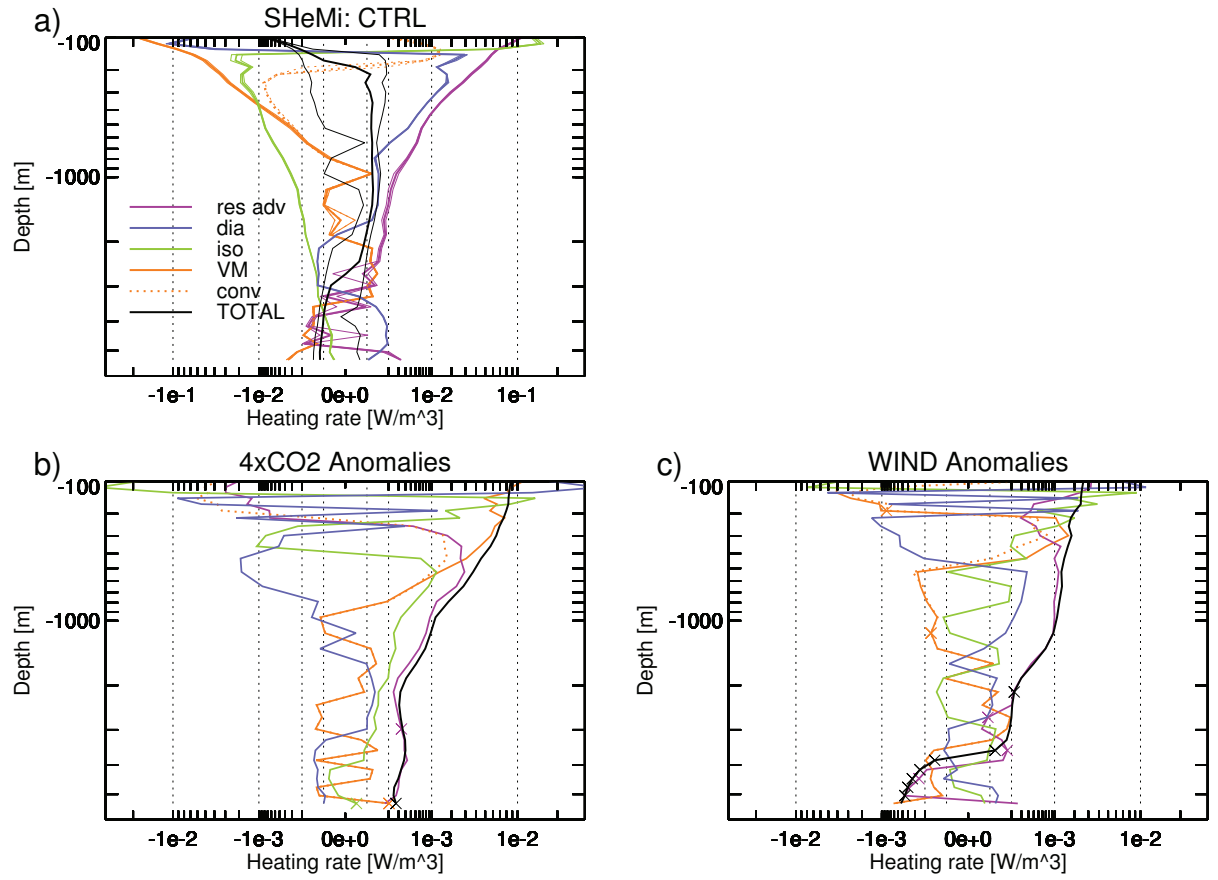


Fig. 6: Horizontally averaged temperature tendency diagnostics for the Southern Hemisphere mid-latitudes for (a) the control run, (b) the 4xCO2 anomalies and (c) the WIND anomalies. Otherwise as Fig. 5.

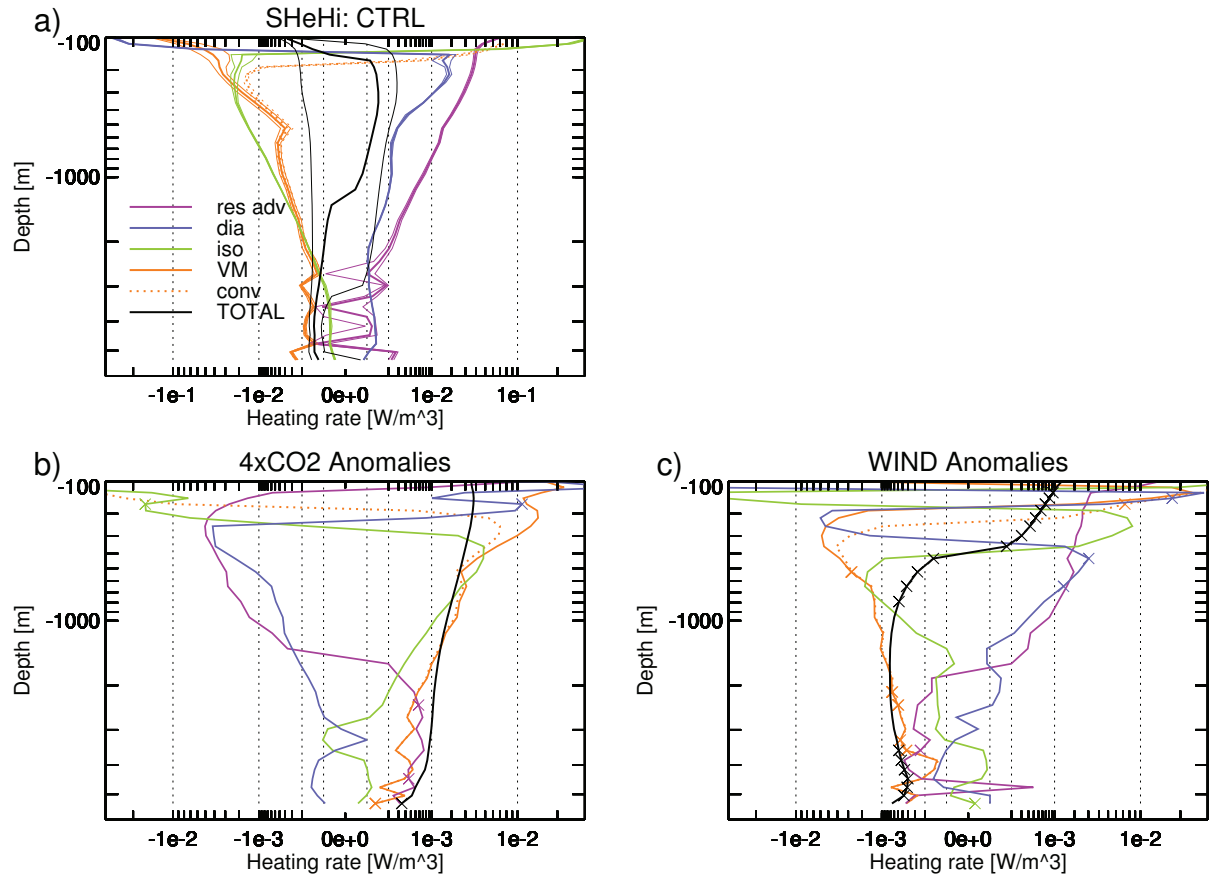


Fig. 7: Horizontally averaged temperature tendency diagnostics for the Southern Hemisphere high latitudes for (a) the control run, (b) the 4xCO2 anomalies and (c) the WIND anomalies. Otherwise as Fig. 5.

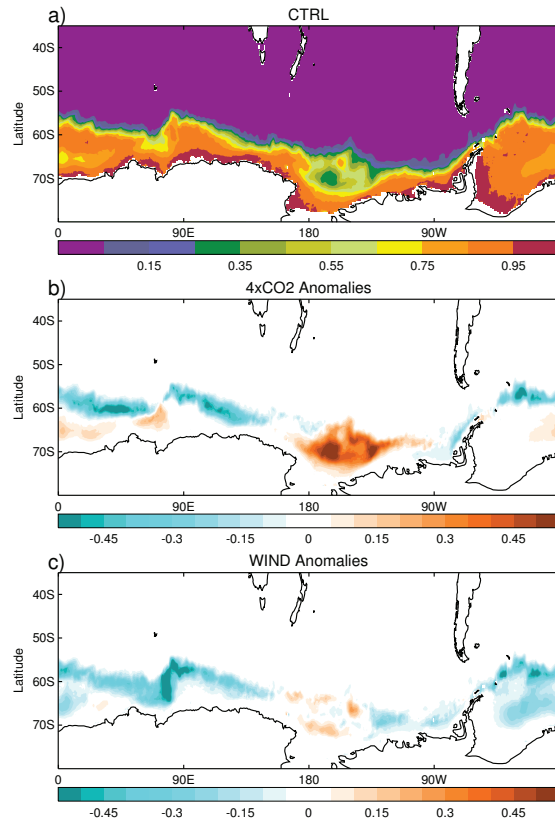


Fig. 8: September sea ice cover (in fractions) in (a) the control run, and anomalies of (b) 4xCO2 and (c) WIND.

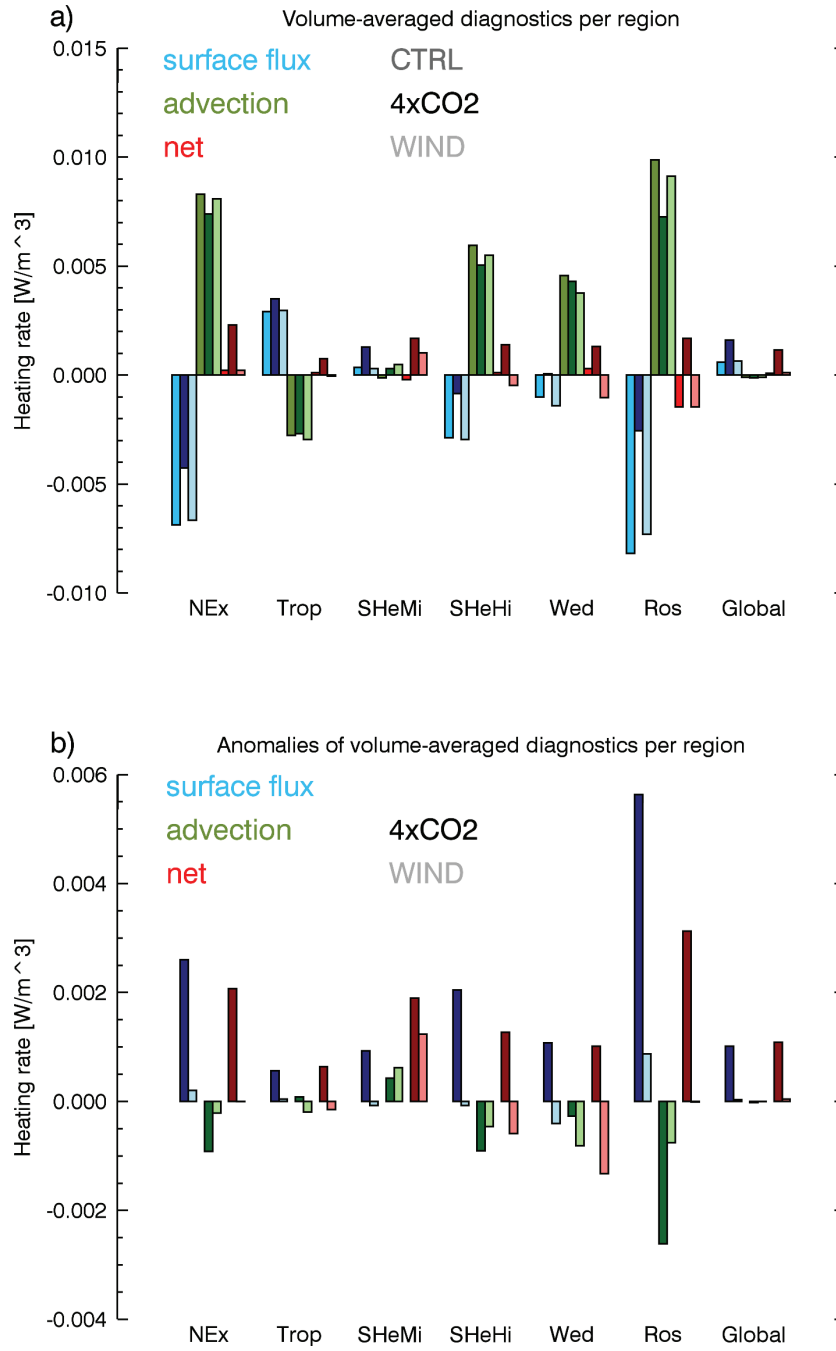


Fig. 9: Overview plot for the most relevant heat uptake processes in the regions of interest discussed in the text. The regions are defined in sec. 4. In (a), each region has three groups of three bars. Each group is colour coded according to the process it represents. In each group, the main colour comes in three hues, where the first bar is for CTRL, the second for 4xCO2 and the third for WIND. Each single bar gives the heating rate for a specific region, process and run. (b) shows the anomalies of the perturbation runs. Therefore, in each group, the main colour comes in two hues, where the first bar is for 4xCO2 (dark hue) and the second for WIND (light hue).

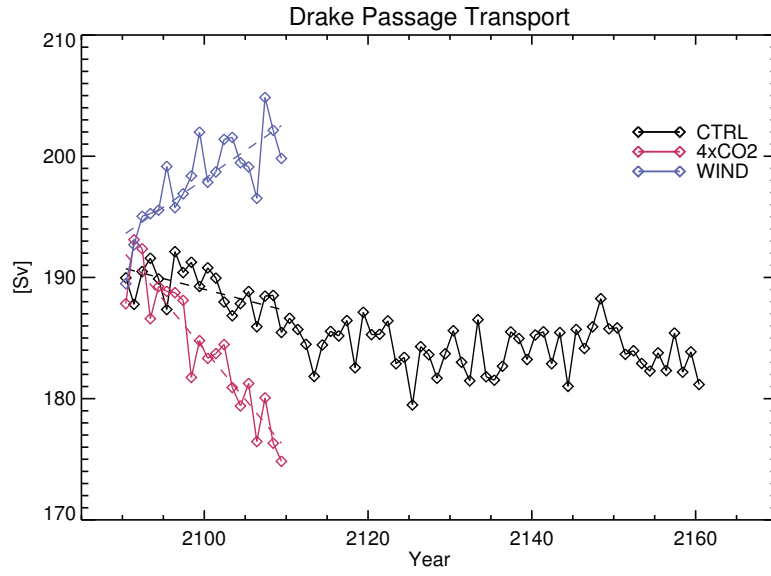


Fig. 10: Drake Passage transport in Sverdrup ($1 \text{ Sv} = 10^6 \text{ m}^3 \text{ s}^{-1}$) in the three HiGEM1.2 runs. Dashed lines: trend estimates over 20 years.

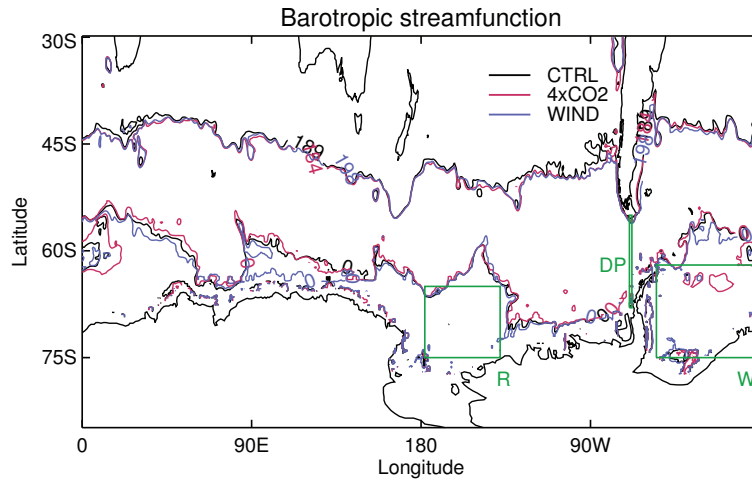


Fig. 11: Barotropic streamfunction contours (20-year average) in Sverdrup ($1 \text{ Sv} = 10^6 \text{ m}^3 \text{ s}^{-1}$) in the three HiGEM1.2 runs. Plotted are the minimum and maximum contours going through Drake Passage for each run. The minimum is 0 Sv by definition. The maxima are 189 Sv for CTRL, 184 Sv for 4xCO2 and 198 Sv for WIND. In addition, the -50 Sv contour has been plotted and shows, around 0°E and 60°S , the increase of the Weddell Gyre in 4xCO2.

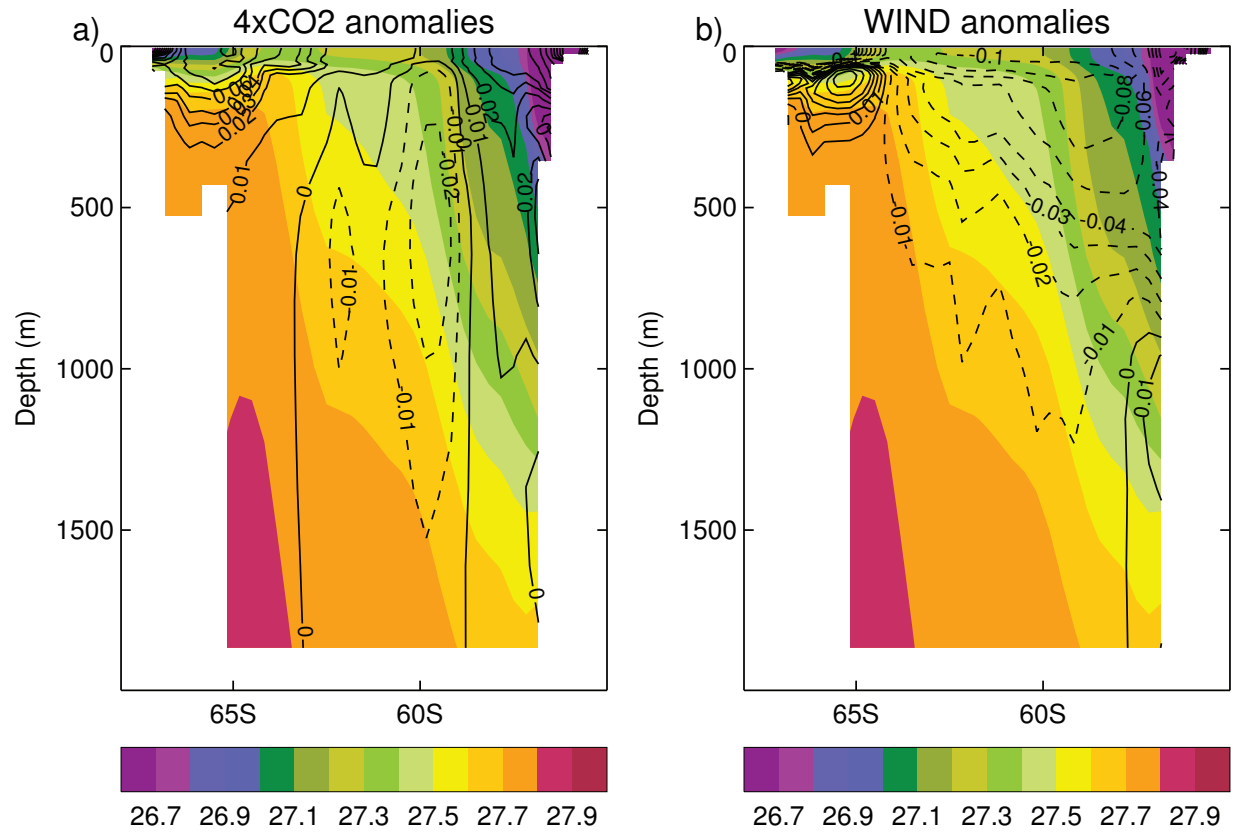


Fig. 12: Zonal average of potential density (shaded, in σ_2 units) and its anomaly (contours) in the Drake Passage region. (a) Anomalies of 4xCO₂, (b) anomalies of WIND. Solid contours indicate positive density anomalies and dashed contours indicate negative anomalies. In 4xCO₂ the isopycnals across the Drake Passage in the top ~1000 m flatten, while in WIND they steepen.

References

- Banks HT, Gregory JM (2006) Mechanisms of ocean heat uptake in a coupled climate model and the implications for tracer based predictions of ocean heat uptake. *Geophys Res Lett* 33:L07608, DOI 10.1029/2005GL025352
- Bouttes N, Gregory J, Kuhlbrodt T, Suzuki T (2012) The effect of windstress change on future sea level change in the Southern Ocean. *Geophys Res Lett* 39(23), DOI 10.1029/2012GL054207
- Brierley CM, Collins M, Thorpe AJ (2010) The impact of perturbations to ocean-model parameters on climate and climate change in a coupled model. *Clim Dyn* 34:325–343, DOI 10.1007/s00382-008-0486-3
- Cai W, Cowan T, Godfrey S, Wijffels S (2010) Simulations of processes associated with the fast warming rate of the southern midlatitude ocean. *J Clim* 23:197–206, DOI 10.1175/2009JCLI3081.1
- Church JA, White NJ, Konikow LF, Domingues CM, Cogley JG, Rignot E, Gregory JM, van den Broeke MR, Monaghan AJ, Velicogna I (2011) Revisiting the Earth's sea-level and energy budgets from 1961 to 2008. *Geophys Res Lett* 38:L18601, DOI 10.1029/2011GL048794
- Downes S, Hogg A (2013) Southern Ocean circulation and eddy compensation in CMIP5 models. *J Clim* 26:7198–7220, DOI 10.1175/JCLI-D-12-00504.1
- Dufresne JL, Bony S (2008) An assessment of the primary sources of spread of global warming estimates from coupled atmosphere-ocean models. *J Clim* 21(19):5135–5144, DOI 10.1175/2008JCLI2239.1
- Eden C, Greatbatch RJ (2009) A diagnosis of isopycnal mixing by mesoscale eddies. *Ocean Modelling* 27:98–106, DOI 10.1016/j.ocemod.2008.12.002
- Exarchou E, Kuhlbrodt T, Gregory JM, Smith RS (2015) Ocean heat uptake processes: a model intercomparison. *J Clim* 28(2):887–908, DOI 10.1175/JCLI-D-14-00235.1
- Farneti R, Delworth TL, Rosati AJ, Griffies SM, Zeng F (2010) The role of mesoscale eddies in the rectification of the Southern Ocean response to climate change. *J Phys Oceanogr* 40:1539–1557, DOI 10.1175/2010JPO4353.1
- Frankcombe LM, Spence P, Hogg AM, England MH, Griffies SM (2013) Sea level changes forced by Southern Ocean winds. *Geophys Res Lett* 40:1–6, DOI 10.1002/2013GL058104
- Gent PR, McWilliams JC (1990) Isopycnal mixing in ocean circulation models. *J Phys Oceanogr* 20:150–155
- Gnanadesikan A, Slater R, Swathi PS, Vallis GK (2005) The energetics of ocean heat transport. *J Clim* 18:2604–2616
- Good P, Gregory JM, Lowe JA (2011) A step-response simple climate model to reconstruct and interpret AOGCM projections. *Geophys Res Lett* 38:L01703, DOI 10.1029/2010GL045208
- Good P, Ingram W, Lambert FH, Lowe JA, Gregory JM, Webb MJ, Ringer MA, Wu P (2012) A step-response approach for predicting and understanding non-linear precipitation changes. *Clim Dyn* 39:2789–2803, DOI 10.1007/s00382-012-1571-1
- Graham RM, de Boer AM, Heywood KJ, Chapman MR, Stevens DP (2012) Southern Ocean fronts: Controlled by wind or topography? *J Geophys Res* 117:C08018, DOI 10.1029/2012JC007887
- Gregory JM (2000) Vertical heat transports in the ocean and their effect on time-dependent climate change. *Clim Dyn* 16(7):501–515, DOI 10.1007/s003820000059

- Gregory JM, Forster PM (2008) Transient climate response estimated from radiative forcing and observed temperature change. *J Geophys Res* 113:D23105, DOI 10.1029/2008JD014050
- Griffies SM, Gnanadesikan A, Pacanowski RC, Larichev VD, Dukowicz JK, Smith RD (1998) Isonutral diffusion in a z-coordinate ocean model. *J Phys Oceanogr* 28:805–830
- Griffies SM, Winton M, Anderson WG, Benson R, Delworth TL, Dufour CO, Dunne JP, Goddard P, Morrison AK, Rosati A, Wittenberg AT, Yin J, Zhang R (2015) Impacts on ocean heat from transient mesoscale eddies in a hierarchy of climate models. *J Clim* 28(3):952–977, DOI 10.1175/JCLI-D-14-00353.1
- Heuzé C, Heywood KJ, Stevens DP, Ridley JK (2013) Southern Ocean bottom water characteristics in CMIP5 models. *Geophys Res Lett* 40:1–6, DOI 10.1002/grl.50287
- Hieronymus M, Nycander J (2013) The budgets of heat and salinity in NEMO. *Ocean Modelling* 67:28–38, DOI 10.1016/j.ocemod.2013.03.006
- Huang B, Stone PH, Sokolov AP, Kamenkovich IV (2003a) The deep-ocean heat uptake in transient climate change. *J Clim* 16:1352–1363
- Huang B, Stone PH, Sokolov AP, Kamenkovich IV (2003b) Ocean heat uptake in transient climate change: mechanisms and uncertainty due to subgrid-scale eddy mixing. *J Clim* 16:3344–3356
- Kirkman IV CH, Bitz CM (2011) The effect of the sea ice freshwater flux on Southern Ocean temperatures in CCSM3: deep-ocean warming and delayed surface warming. *J Clim* DOI 10.1175/2010JCLI3625.1
- Kuhlbrodt T, Gregory JM (2012) Ocean heat uptake and its consequences for the magnitude of sea level rise and climate change. *Geophys Res Lett* 39:L18608, DOI 10.1029/2012GL052952
- Large W, McWilliams J, Doney S (1994) Oceanic vertical mixing: A review and a model with a nonlocal boundary layer parameterization. *Rev Geophys* 32(4):363–403, DOI 10.1029/94RG01872
- Lee MM, Nurser AJG, Coward AC, de Cuevas BA (2007) Eddy advective and diffusive transports of heat and salt in the Southern Ocean. *J Phys Oceanogr* 37:1376–1393, DOI 10.1175/JPO3057.1
- Locarnini RA, Mishonov AV, Antonov JJ, Boyer TP, Garcia HE, Baronova OK, Zweng MM, Johnson DR (2006) World Ocean Atlas 2009. U.S. Government Printing Office, Washington, D.C., US, NOAA Atlas NESDIS 68, vol 1, p 184
- Manabe S, Bryan K, Spelman M (1990) Transient response of a global ocean-atmosphere model to a doubling of atmospheric carbon dioxide. *J Phys Oceanogr* 20:722–749
- Marshall J, Radko T (2003) Residual-mean solution for the Antarctic Circumpolar Current and its associated overturning circulation. *J Phys Oceanogr* 33:2341–2354
- Mazloff M, Heimbach P, Wunsch C (2010) An eddy-permitting Southern Ocean state estimate. *J Phys Oceanogr* 40:880–899
- Megann A, Storkey D, Aksenov Y, Alderson S, Calvert D, Graham T, Hyder P, Siddorn J, Sinha B (2014) GO5.0: the joint NERC Met Office NEMO global ocean model for use in coupled and forced applications. *Geoscientific Model Development* 7:1069–1092, DOI 10.5194/gmd-7-1069-2014
- Meijers A, Shuckburgh E, Bruneau N, Sallee JB, Bracegirdle T, Wang Z (2012) Representation of the Antarctic Circumpolar Current in the CMIP5 climate models and future changes under warming scenarios. *J Geophys Res* 117:C12008, DOI 10.1029/2012JC008412
- Morrison AK, Saenko OA, Hogg AM, Spence P (2013) The role of vertical eddy transport in Southern Ocean heat uptake. *Geophys Res Lett* 40, DOI 10.1002/2013GL057706

- 932 Munk W, Wunsch C (1998) Abyssal recipes II: energetics of tidal and wind mixing. *Deep-*
933 *Sea Research I* 45:1977–2010
- 934 Pardaens AK, Gregory JM, Lowe JA (2011) A model study of factors influencing projected
935 changes in regional sea level over the 21st century. *Clim Dyn* 36(9-10):2015–2033, DOI
936 10.1007/s00382-009-0738-x
- 937 Peters H, Gregg MC, Sanford TB (1995) Detail and scaling of turbulent overturns
938 in the Pacific equatorial undercurrent. *J Geophys Res* 100(C9):18,349–18,368, DOI
939 10.1029/95JC01360
- 940 Rahmstorf S (1993) A fast and complete convection scheme for ocean models. *Ocean Mod-*
941 *elling* 101:9–11
- 942 Roberts MJ, Marshall D (1998) Do we require adiabatic dissipation schemes in eddy-
943 resolving ocean models? *J Phys Oceanogr* 28:2050–2063
- 944 Sen Gupta A, Muir LC, Brown JN, Phipps SJ, Durack PJ, Monselesan D, Wijffels SE
945 (2012) Climate drift in the CMIP3 models. *J Clim* 25:4621–4640, DOI 10.1175/JCLI-
946 D-11-00321.1
- 947 Shaffrey LC, Stevens I, Norton WA, Roberts MJ, Vidale PL, Harle JD, Jrrar A, Stevens
948 DP, Woodage MJ, Demory ME, Donners J, Clark DB, Clayton A, Cole JW, Wilson SS,
949 Connolley WM, Davies TM, Iwi AM, Johns TC, King JC, New AL, Slingo JM, Slingo
950 A, Steenman-Clark L, Martin GM (2009) U.K. HiGEM: The new U.K. high-resolution
951 global environment model—Model description and basic evaluation. *J Clim* 22:1861–
952 1896, DOI 10.1175/2008JCLI2508.1
- 953 Sigmond M, Reader MC, Fyfe JC, Gillett NP (2011) Drivers of past and future Southern
954 Ocean change: stratospheric ozone versus greenhouse gas impacts. *Geophys Res Lett*
955 38:L12601, DOI 10.1029/2011GL047120
- 956 Wang Z, Kuhlbrodt T, Meredith MP (2011) On the response of the Antarctic Circum-
957 polar Current transport to climate change in coupled climate models. *J Geophys Res*
958 116:C08011, DOI 10.1029/2010JC006757
- 959 Wolfe CL, Cessi P, McClean JL, Maltrud ME (2008) Vertical heat transport in eddying ocean
960 models. *Geophys Res Lett* 35:L23605, DOI 10.1029/2008GL036138
- 961 Yin J (2012) Century to multi-century sea level rise projections from CMIP5 models. *Geo-*
962 *phys Res Lett* 39(17), DOI 10.1029/2012GL052947
- 963 Yin J, Griffies SM, Stouffer RJ (2010) Spatial variability of sea level rise in twenty-first
964 century projections. *J Clim* 23:4585–4607